PAPER

Stability analysis of secondary modes, driven by the phase space island

IOP Publishing | International Atomic Energy Agency Nuclear Fusion

Nucl. Fusion **59** (2019) 086010 (17pp) https://doi.org/10.1088/1741-4326/ab2077

Stability analysis of secondary modes, driven by the phase space island

A.V. Dudkovskaia[1], X. Garbet[2], M. Lesur[3] and H.R. Wilson[1,4]

[1] York Plasma Institute, Department of Physics, University of York, Heslington, York YO10 5DD, United Kingdom of Great Britain and Northern Ireland
[2] CEA, IRFM, F13108 St. Paul-lez-Durance cedex, France
[3] Université de Lorraine, CNRS, IJL, F-54000 Nancy, France
[4] CCFE, Culham Science Centre, Abingdon, Oxon OX14 3DB, United Kingdom of Great Britain and Northern Ireland

E-mail: avd512@york.ac.uk

Received 28 January 2019, revised 11 April 2019
Accepted for publication 9 May 2019
Published 21 June 2019

Abstract

We present a new theoretical approach, based on the Hamiltonian formalism, to investigate the stability of islands in phase space, generated by trapping of energetic particles (EPs) in plasma waves in a tokamak. This approach is relevant to MHD modes driven by EPs (EP-MHD) such as toroidal Alfvén eigenmodes (TAEs), EP-driven geodesic acoustic modes (EGAMs) or fishbones. A generic problem of a single isolated EP-MHD mode is equivalent to and hence can be replaced by a 2D Hamiltonian dynamics in the vicinity of the phase space island. The conventional Langmuir wave/bump-on-tail problem is then used as a representative reduced model to describe the dynamics of the initial EP-MHD.

Solving the Fokker–Planck equation in the presence of pitch angle scattering, velocity space diffusion and drag and retaining plasma drifts in a model, we find a 'perturbed' equilibrium, associated with these phase space islands. Its stability is then explored by addressing the Vlasov/Fokker–Planck–Poisson system. The Lagrangian of this system provides the dispersion relation of the secondary modes and allows an estimate of the mode onset. The secondary instabilities have been confirmed to be possible but under certain conditions on the primary island width and in a certain range of mode numbers. The threshold island width, below which the mode stability is reached, is calculated. The secondary mode growth rate is found to be maximum when the associated resonant velocity approaches the boundary of the primary island. This, in turn, leads to a conclusion that the onset of the secondary mode can be prevented provided the primary wave number is the lowest available.

Keywords: secondary modes, phase space island, energetic particles, stability analysis, bump-on-tail instability, toroidal Alfven eigenmodes, Hamiltonian formalism

(Some figures may appear in colour only in the online journal)

1. Introduction

Particle-wave interaction plays a crucial role in a variety of applications. It is particularly important in burning tokamak plasmas since fast particles are required to provide additional heating and current drive in a reactor. Energetic particles (EPs) can be produced by neutral beam injection (NBI) or radio frequency (RF) heating, as well as fusion reactions themselves. These fast particles can drive Alfvén eigenmodes, which, in turn, may lead to detrimental particle losses. Since alpha particles are considered as the main heating source in a fusion reactor, their losses need to be mitigated or prevented in an optimal scenario. In a tokamak, various nonlinear regimes can be gathered under the umbrella of this bump-on-tail instability [1–3]. In its simplest version, the bump-on-tail instability can be modelled by a background of thermal electrons with a Maxwellian velocity distribution, neutralized by steady ions, while fast electrons are described by a shifted Maxwellian,

localized near a beam velocity, V_b. The problem is 2D, i.e. one spatial direction, x, and the corresponding velocity variable, V. If the beam velocity is large enough, the electron distribution function exhibits a positive slope in the vicinity of V_b, which is prone to instabilities. In its original version, these modes are Langmuir waves, but are akin to Alfvén modes, driven by a population of fast particles in a tokamak [4–6]. A bump-on-tail instability is driven linearly via a wave-particle resonance, which occurs when the particle velocity matches the mode phase velocity, $V_{\rm ph} = \omega_0/k_0$, where ω_0 is the mode pulsation and k_0 is its wave number. A single mode (ω_0, k_0) evolves nonlinearly in various ways depending on the dissipation terms (distribution function and field) and the strength of the drive. The different behaviors (steady, periodic, chaotic and chirping) have been widely studied in the past, and led to phase diagrams that provide the type of dynamics depending on plasma parameters [7, 8]. Saturation towards a steady state, which is paradigmatic when dissipation is high enough, is due to the formation of an island near the resonant velocity, $V = V_{\rm ph}$. The distribution function flattens within the island, thus decreasing the drive. Saturation occurs when the residual drive matches the dissipation rate, which is large near the island separatrix, where the gradients of the distribution function are steep. This process leads to the formation of a plateau near $V = V_{\rm ph}$ [9]. We also note that saturation is possible in the collisionless regime via the formation of a plateau in velocity space within the island, and the onset of O'Neil–Mazitov oscillations [10–12]—we will however restrict the analysis in the present work to the case where dissipation remains finite.

Steady solutions are no longer allowed when the dissipation rate decreases. One interesting behavior is called frequency chirping, the name of which is self-explanatory. Frequency chirping is ubiquitous in tokamaks for toroidal Alfvèn eigenmodes (TAEs) or fishbones [13–15]. The explanation, proposed within the framework of the bump-on-tail problem, involves the formation of clumps and holes in phase space. The motion of a clump/hole pair is associated with a time dependence of the mode frequency, i.e. chirping [2]. We note that other explanations have been proposed in the limit of strong drive [3]. The limit of weak drive only will be considered here. It should be highlighted that the model, described in [2], also called the 'Berk–Breizman' model, addresses the asymptotic behavior of a clump/hole pair dynamics. The mechanism that leads to the formation of the clump/hole pair is still elusive. One mechanism was proposed by Lilley and Nyqvist [16], where the clump/hole pair appears because of the onset of secondary instabilities that occur near the nonlinear structure, associated with a 'primary' mode. The primary mode here is an unstable wave (ω_0, k_0), that evolved into a nonlinear quasi-saturated state, associated with a plateau of the distribution function near the resonant velocity, $V = V_{\rm ph}$. The steepening of the distribution at the edges of the plateau drives, in turn, secondary instabilities, which are identified as negative energy waves in [16]. It should be stressed here that in this work, the plateau is a band in the velocity space V, and hence does not depend on the spatial coordinate x. However, the primary mode is expected to evolve towards the formation of an island in phase space [17]. A plateau then forms inside the island region, bounded by the separatrix, in the vicinity of which secondary modes are expected to appear. Intrinsically, this is a 2D problem in phase space, (x, V). The onset of secondary instabilities near the island in phase space is the question that is addressed here.

The island in phase space can be treated as a special case of a BGK mode, named after Bernstein, Greene and Kruskal, who predicted that BGK modes belong to a large class of nonlinear solutions of the Vlasov–Poisson problem [18]. Hence, the existence of secondary instabilities close to the island in phase space is related to the question of whether BGK modes are stable or not. One important difference though is that BGK modes are usually investigated in the collisionless limit, whereas collisions have an important influence on the saturated primary mode in the present work. An important theorem that applies to the bump-on-tail problem states that the BGK saturated mode is unstable [19]. A secondary instability generically appears in the form of a subharmonic mode with a wave number that is half the wave number of the primary BGK mode. The proof is given for a primary mode amplitude that is small enough, i.e. a situation not too far away from marginal stability. Nevertheless, the regime is nonlinear in essence since particles, trapped in the primary BGK mode, are accounted for. The theorem predicts instability, but does not provide a quantitative growth rate of the secondary mode. The situation is less clear for numerical simulations and related analytic work, since secondary instabilities are predicted and found under certain conditions only [17, 20, 21]. Indeed, it appears in [20, 21] that at least three beams are required to obtain instability . This result comes from a linear stability analysis and numerical simulations. More recently the stability of BGK modes has been numerically investigated for the bump-on-tail problem [17]. It was found that the onset of secondary instabilities is not systematic. When a secondary mode appears, it is usually a subharmonic of the primary one, in agreement with the aforementioned theorem [19]. However, it appears in practice that secondary instabilities are, in fact, linearly weakly unstable [17]. Therefore, the stability of BGK states seems to be connected to the linear stability properties of the unperturbed state, as highlighted in [19, 21]. This is not exactly what is looked for as ideally the initial state should be such that a *single* primary mode is linearly unstable, while secondary modes are fully stable. Nevertheless, the nonlinear strengthening of a mode that is initially weakly unstable is certainly of interest for practical purposes. It should be underlined here that most analytic calculations do not take into account the island shape of the primary equilibrium, i.e. most assume a small island width, which is, in fact, equivalent to a linear stability analysis of the unperturbed state.

The present work investigates the stability of a dissipative primary equilibrium, i.e. situations where a plateau of the distribution function forms within the primary island, without any restriction on the island width, and therefore on the distance to marginal stability. Hence this calculation applies to large island widths, i.e. fully nonlinear situations. The primary equilibrium is determined by the solution of the Fokker–Planck equation, i.e. with collisions, accounting for both diffusion and drag. A dispersion relation is then derived.

Two forms have been obtained. In the first one, the distribution function appears only via its average over the island structure. This dispersion relation applies to numerical simulations, where a single secondary mode is allowed to grow. A second dispersion relation has also been determined, which fully accounts for the details of the distribution function. It appears that the onset of secondary modes depends sensitively on the width of the island. Typically the instability growth rate becomes positive above a critical island width, reaches a maximum, then decreases with increasing island width. Stability occurs above a second critical island width. This result is in line with time dependent numerical simulations, which find that the stability of a primary mode depends sensitively on the island width. Basically the growth rate is optimum when the steepening of the distribution function near the island separatrix matches the phase velocity of the secondary mode.

The remainder of the paper is organized as follows. Section 2 states the problem. The primary nonlinear equilibrium is computed in section 3. Section 4 provides the analytic derivation of the dispersion relation for secondary modes and addresses numerical solutions of this dispersion relation, as well as initial value solutions. A conclusion follows.

2. Position of the problem

To seek secondary instabilities, we address the conventional Vlasov/Fokker–Planck–Poisson system, i.e. a set of Vlasov/Fokker–Planck equations

$$\frac{\partial f_j}{\partial t} + V_{\parallel}\nabla_{\parallel} f_j + \boldsymbol{V}_{E\times B}\cdot\nabla f_j + \boldsymbol{V}_b\cdot\nabla f_j - \frac{eZ_j}{m_j V}\left[V_{\parallel}\nabla_{\parallel}\Phi + \boldsymbol{V}_b\cdot\nabla\Phi\right]\frac{\partial f_j}{\partial V} = C_j\left(f_j\right) + S \tag{1}$$

for each particle species, j, coupled to Poisson's equation

$$\varepsilon_0\nabla^2\Phi = -\sum_j eZ_j\int_{\mathbb{R}} f_j \mathrm{d}\boldsymbol{V}. \tag{2}$$

Here $\parallel$ denotes a vector component along the magnetic field lines, $\nabla_{\parallel} = \boldsymbol{b}\cdot\boldsymbol{\nabla}$, $\boldsymbol{b} = \boldsymbol{B}/B$. $\boldsymbol{V}_{E\times B}$ and $\boldsymbol{V}_b$ are the $\boldsymbol{E}\times\boldsymbol{B}$ and magnetic drift contributions. Φ is the electrostatic potential; eZ_j and m_j are the particle charge and mass, respectively. The right hand side, written as a sum of the collision operator, C_j, and a source term, S, is to be introduced below. A system of three particle species is considered: j in equations (1) and (2) is used for thermal electrons and ions, as well as a population of EPs, i.e. fast electrons/ions that trigger the bump-on-tail instability. In a toroidal set of coordinates, the particle distribution function, f_j, is to be understood as $f_j = f_j\left(t,\psi,\vartheta,\zeta,\boldsymbol{V}\right)$. ψ is the poloidal flux function; ϑ and ζ are the poloidal and helical angles, respectively. ζ is defined as $m_0\vartheta - n_0\varphi - \omega_0 t$, where m_0/n_0 are the poloidal/toroidal primary mode number, φ is the toroidal angle, and ω_0 is the primary mode frequency. Equation (1) can be rewritten as a pair of Hamilton's equations for a set of angular and action variables, $\{\boldsymbol{\alpha},\boldsymbol{J}\}$. For a tokamak plasma, the action vector components are represented by three adiabatic invariants of charged particle motion. Introducing a single perturbation, associated with the island in phase space, we have $\mathcal{H}_0\left(\boldsymbol{J},\boldsymbol{\alpha},t\right) = \mathcal{H}_{00}\left(\boldsymbol{J}\right) + h\cos\left(\boldsymbol{n}\boldsymbol{\alpha} - \omega_0 t\right)$ for the full primary Hamiltonian. Here $\mathcal{H}_{00}$ is the unperturbed Hamiltonian, i.e. in the absence of the island, and $\boldsymbol{n} = (n_1, n_2, n_3)$ is a triplet of integers. Setting $\xi = \boldsymbol{n}\boldsymbol{\alpha} - \omega_0 t$, we define a resonant surface by $\sum_{i=1}^{3} n_i\Omega_i\left(\boldsymbol{J}\right) = \omega_0$ with $\mathrm{d}\boldsymbol{\alpha}/\mathrm{d}t = \boldsymbol{\Omega}\left(\boldsymbol{J}\right)$. Then the action vector becomes $\boldsymbol{J} = \boldsymbol{J}_{\mathrm{res}} + \boldsymbol{n}I$ in the vicinity of the resonant surface, where $\boldsymbol{J}_{\mathrm{res}}$ is a vector that lies on the resonant surface and I measures the corresponding distance to it (see figure 1). Then it can be easily verified that $\mathcal{H}_0\left(\boldsymbol{J},\boldsymbol{\alpha},t\right) = \mathcal{H}_{00}\left(\boldsymbol{J}_{\mathrm{res}}\right) + CI^2/2 + h\cos\xi$, where C is the Hessian of the Hamiltonian on the resonant surface. To simplify the analysis below, we take h slowly varying over the island width. Setting $p = CI$, we obtain

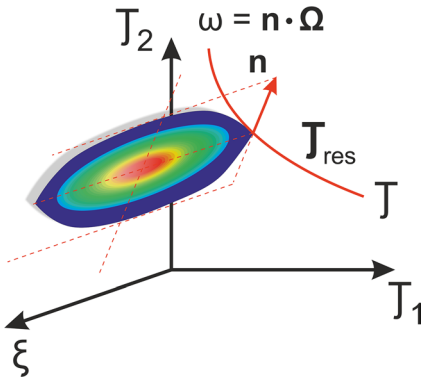

Figure 1. A phase space island near the resonant surface, $\boldsymbol{n}\cdot\boldsymbol{\Omega}(\boldsymbol{J}) = 0$.

$$H_0 = p^2/2 - \omega_b^2\cos\xi \tag{3}$$

for a new total primary Hamiltonian. The bounce frequency of deeply trapped particles (i.e. particles trapped in phase space), ω_b, has been defined according to $\omega_b^2 = -Ch$. Here we note that any 6D dynamics in phase space can be reduced to a 2D phase space island dynamics, provided two invariants of motion lie on the resonant surface.

In the slab geometry in the absence of tokamak drifts, equation (1) simply reads

$$\frac{\partial f_j}{\partial t} + V\frac{\partial f_j}{\partial x} - \frac{eZ_j}{m_j}\frac{\partial\Phi}{\partial x}\frac{\partial f_j}{\partial V} = C_j\left(f_j\right) + S. \tag{4}$$

Equation (1)/equation (4) is to be solved for f_j, a time dependent particle distribution function, considered as a function of position, $\{\psi,\vartheta,\zeta\}/x$, and velocity, $\boldsymbol{V}/V$. Φ is a function of position and time. For simplicity, let us restrict the analysis to the (t,x) plane. We assume that a primary wave has been developed and saturated in the form of an island and that the corresponding potential is $\Phi\left(x,t\right) = \Phi_0\cos\left(k_0 x - \omega_0 t\right)$. It is then convenient to work in a wave reference frame and introduce a new spatial variable $\xi = k_0 x - \omega_0 t$ that is conjugated to a momentum, $p = \partial\xi/\partial t = k_0 V - \omega_0$. Hence, the Hamiltonian in this set of variables becomes $H_0\left(x,V\right) = \left(k_0 V - \omega_0\right)^2/2 - k_0^2\left(eZ_j/m_j\right)\Phi_0\cos\left(k_0 x - \omega_0 t\right)$. It is an invariant of motion and is equivalent to p as a variable in velocity space, provided the sign of p, noted σ_p, is

kept as an extra variable. Defining the bounce frequency at the deeply trapped end as $\omega_b^2 = k_0^2 eZ_j\Phi_0/m_j$, we again write equation (3) for the full primary Hamiltonian in the (p,ξ) plane. Extending this to the toroidal geometry, we replace $H_0(x,V)$ with $H_0(\psi,\varphi,\vartheta,\boldsymbol{V}) = V_\parallel^2/2 + \mu B + eZ_j\Phi(\psi,\varphi,\vartheta)$ [22] with $\mu = V_\perp^2/2B$ denoting the magnetic moment, and B being the total magnetic field. The electrostatic potential takes the form $\Phi_0\cos\zeta$ (the ψ dependence of Φ_0 has been neglected for convenience). We underline that the guiding center equations of motion in a tokamak that fully account for the magnetic drifts as well as their reduced slab formulation are allowed to be written in a Hamiltonian form. Thus, from a mathematical point of view any EP-MHD problem, including both the Langmuir wave and the TAE problems, becomes identical in the toroidal and slab geometry, if written in terms of the Hamiltonian function.

Constant H_0 contours in the (p,ξ) plane describe an island-like structure and will be referred to as an island in phase space. A new equilibrium, described by $f_{0,j}$, is to be calculated from the Fokker–Planck equation, which now reads as

$$\frac{\partial f_{0,j}}{\partial t} - \{H_0, f_{0,j}\} = C_j(f_{0,j}) + S. \tag{5}$$

Here curly brackets represent the conventional Poisson bracket, i.e. $\{f,g\} = \frac{\partial f}{\partial\xi}\frac{\partial g}{\partial p} - \frac{\partial f}{\partial p}\frac{\partial g}{\partial\xi}$. Once $f_{0,j}$ is obtained, we can investigate the stability of this new, 'perturbed', equilibrium, i.e. the stability of secondary waves, which we take of the form $\Phi_{k\omega}e^{ikx-i\omega t} + \text{c.c.}$, where k and ω are their wave number and frequency, respectively. In the primary wave frame, these waves become $\Phi_{k\omega}e^{il\xi - i\delta\omega t} + \text{c.c.}$ with $l = k/k_0$ and $\delta\omega = \omega - l\omega_0$. l here is not necessarily an integer. We also need to rewrite equation (2) in an equivalent Lagrangian formulation. If the electrostatic potential takes the form $\Phi(x,t) = \Phi_\omega e^{-i\omega t} + \text{c.c.}$, then the full Hamiltonian and the full EP distribution function read $H(\xi,p) = H_0(\xi,p) + \delta H$ and $f_j(\xi,p) = f_{0,j}(\xi,p) + \delta f_j$ with $\delta H = h_\omega(\xi,p)\,e^{-i\delta\omega t} + \text{c.c.}$ and $\delta f_j = f_{j\omega}(\xi,p)\,e^{-i\delta\omega t} + \text{c.c.}$ Here $H_0(\xi,p)$ and $f_{0,j}(\xi,p)$ correspond to the new primary equilibrium, which will be the subject of section 3, while δH and δf_j are perturbed parts of the Hamiltonian and of the EP distribution function that arise due to the secondary mode occurrence. The amplitude factor is $h_\omega = eZ_j\Phi_\omega$ with $h_\omega(\xi,p) = h_{k\omega}e^{il\xi}$ (kx is to be replaced by $m\vartheta - n\varphi$ in a tokamak extension with m/n being the poloidal/toroidal secondary mode number). Poisson's equation is then equivalent to the state, where the functional

$$\mathcal{L}(\omega) = \varepsilon_0\int_0^L \mathrm{d}x|\nabla\Phi_\omega|^2 - \sum_j eZ_j\int_0^L \mathrm{d}x\int_{\mathbb{R}} f_{j\omega}(\xi,p)\,\Phi_\omega^*(\xi,p)\,\mathrm{d}V \tag{6}$$

is extremum for any variation of Φ_ω^*. Here L is the box length, chosen as a multiple of the primary period, $k_0L = 2\pi j_0$, where j_0 is integer. Thus, we solve $\partial\mathcal{L}/\partial\Phi_\omega^* = 0$ according to Fermat's theorem, and once the solution is found, $\mathcal{L}(\omega) = 0$ provides the dispersion relation for the secondary modes. Redefining the Lagrangian, given by equation (6), to rewrite it in terms of $\{p,\xi\}$, we have

$$\mathcal{L}(\omega,l) = -l^2|h_{k\omega}|^2 + \sum_j \mathcal{L}_j(\omega) \tag{7}$$

with

$$\mathcal{L}_j(\omega) = \omega_{pj}^2\int_{-\pi}^{\pi}\frac{\mathrm{d}\xi}{2\pi}\int_{\mathbb{R}} f_j h_\omega^*\mathrm{d}p. \tag{8}$$

$\mathcal{L}_j$ is the Lagrangian of a given species. The first term in equation (7) is the field contribution to Poisson's equation. Here ω_{pj} is the plasma frequency of a species, $\omega_{pj}^2 = n_j(eZ_j)^2/\varepsilon_0 m_j$, and the particle distribution function is normalized to density of a considered species, n_j, in p coordinates, i.e. $\int_{\mathbb{R}} f_j\mathrm{d}p = 1$. The perturbed Hamiltonian, $h_{k\omega}$, is defined as $h_{k\omega} = k_0^2 eZ_j\Phi_{k\omega}/m_j$. We note that a constant normalization factor has been dropped here. The perturbed distribution function, $f_{j\omega}$, is a solution of the linearized Fokker–Planck equation:

$$-i\delta\omega f_{j\omega} - \{H_0, f_{j\omega}\} = \{h_\omega, f_{0,j}\}. \tag{9}$$

Since $f_{0,j}$ is a non-trivial function of $H_0(p,\xi)$, the Poisson brackets $\{H_0, f_{j\omega}\}$ and $\{h_\omega, f_{0,j}\}$ introduce multiples of the basic harmonic, $l\xi - \delta\omega t$. However far from the island, $H_0 \simeq p^2/2$, and the corresponding solution is trivial. The system then behaves as if primary and secondary waves do not interact. This case is to be applied to thermal particles, provided the thermal resonances occur far from the EP resonances in phase space. The second approach, which we run numerically, consists in keeping the basic harmonics only, so that the Fokker–Planck equation reads

$$-i\delta\omega f_{j\omega} - \{H_0, f_{j\omega}\} = \left\{h_\omega, \langle f_{0,j}\rangle_\xi\right\}. \tag{10}$$

An angular bracket here indicates an average over ξ and will be defined below. Finally, a full nonlinear solution can be obtained by moving from the set of variables $\{\xi,p\}$ to $\{\xi,H_0;\sigma_p\}$ and will be the subject of section 4.

3. Primary equilibrium

To search for the secondary instabilities, we start with a calculation of a new primary equilibrium state, given by $f_{0,j}$. $f_{0,j}$ is a solution of equation (5) and describes the electron/ion response to a single island in phase space, associated with the bump-on-tail instability. As the main electrons and ions are assumed to be Maxwellian, equation (5) is to be solved only for the EP fraction, i.e. fast electrons/ions, whose population is lower compared to the bulk plasma. The combined effect of the source term and the collision operator is written through the Fokker–Planck collision integral that includes collisions on EPs by the thermal, Maxwellian background. The initial form of this collision operator acting on the EP distribution function is taken to be of the form:

$$C_j + S = 2\nu_j\frac{(1-\lambda B)^{1/2}}{B}\frac{\partial}{\partial\lambda}\bigg|_\psi\left[\lambda(1-\lambda B)^{1/2}\frac{\partial}{\partial\lambda}\bigg|_\psi\right] + \frac{1}{V^2}\frac{\partial}{\partial V}\left[V^3\left(\nu_{\text{slow}} + \frac{\nu_\parallel}{2}V\frac{\partial}{\partial V}\right)\right], \tag{11}$$

where ν_j, ν_{slow} and $\nu_{\|}$ are the pitch angle scattering, slowing down and parallel velocity diffusion rates, respectively. λ here is the pitch angle, defined as $2\mu/V^2$. Following the Berk and Breizman paper [23, 24], we project this Fokker–Planck operator on the resonant phase space surface to replace it by a combination of operators in p space. This reduces the collision integral dimension from 2D to 1D in velocity space. The Jacobian of this coordinate transformation is given in [23]. After this procedure, we come to

$$C_j\left(f_{0,j}\right)+S=D_p\left.\frac{\partial^2}{\partial p^2}\right|_{\xi}\left(f_{0,j}-f_{eqm,j}\right)+\nu_{f,p}\left.\frac{\partial}{\partial p}\right|_{\xi}\left(f_{0,j}-f_{eqm,j}\right). \tag{12}$$

Here D_p and $\nu_{f,p}$ are the diffusion and dynamical friction (i.e. slowing down) coefficients in p space, related to the diffusion $\nu_{d,V}$ and friction $\nu_{f,V}$ rates in velocity space via $D_p=\nu_{d,V}^3(k_0/k)^2$ and $\nu_{f,p}=\nu_{f,V}^2(k_0/k)$. $f_{eqm,j}$ is the unperturbed distribution function, i.e. in the absence of the phase space island, which appears as a dotted line in figure 3. The Vlasov part of the Fokker–Planck equation [25] is

$$\frac{\mathrm{d}f_{0,j}}{\mathrm{d}t}\equiv\frac{\partial f_{0,j}}{\partial t}-\tau\left[\partial_t H_0-\left\langle\partial_t H_0\right\rangle_{\xi}\right]\frac{\partial f_{0,j}}{\partial J}+p\frac{\partial f_{0,j}}{\partial\xi} \tag{13}$$

with J being the action variable, defined as $J\left(H_0,t\right)=\oint\frac{\mathrm{d}\xi}{2\pi}p\left(t,\xi,H_0;\sigma_p\right)$, and τ denoting the bounce period, $\tau=\oint\frac{\mathrm{d}\xi}{2\pi}p^{-1}\left(t,\xi,H_0;\sigma_p\right)$ (an angular bracket denotes the ξ-averaging procedure and is to be introduced later in this section). Working in the wave reference frame and seeking the time-independent solution, we reduce a set of equations (5), (12) and (13) to

$$\begin{aligned}p\left(\xi,H_0;\sigma_p\right)\left.\frac{\partial f_{0,j}}{\partial\xi}\right|_{H_0}&=D_p p^2\left(\xi,H_0;\sigma_p\right)\left.\frac{\partial^2}{\partial H_0^2}\right|_{\xi}\left(f_{0,j}-f_{eqm,j}\right)\\&+\left[D_p+\nu_{f,p}p\left(\xi,H_0;\sigma_p\right)\right]\left.\frac{\partial}{\partial H_0}\right|_{\xi}\left(f_{0,j}-f_{eqm,j}\right).\end{aligned} \tag{14}$$

Here p has been replaced by a pair $\{H_0;\sigma_p\}$. It is convenient to define a new distribution function, $g_{0,j}$, as $f_{0,j}-f_{eqm,j}$ to measure a shift from the equilibrium state. To solve equation (14) for $g_{0,j}$, we define a small parameter $\delta=\max\left(D_p/\omega_b^3,\nu_{f,p}/\omega_b^2\right)\ll 1$, which implies weak collisional dissipation. Treating the system perturbatively, we apply an expansion $g_{0,j}=\sum_\alpha g_{0,j}^{(\alpha)}\delta^\alpha$ to obtain

$$\left.\frac{\partial g_{0,j}^{(0)}}{\partial\xi}\right|_{H_0}=0 \tag{15}$$

to 0th order. Here we learn that $g_{0,j}^{(0)}$ is ξ-independent at any fixed H_0, i.e. $g_{0,j}^{(0)}=g_{0,j}^{(0)}\left(H_0;\sigma_p\right)$. Proceeding to next order by introducing collisions, we obtain an exact form of $g_{0,j}^{(0)}$ from the collisional constraint. The $O\left(\delta^1\right)$ equation reads

$$\begin{aligned}p\left(\xi,H_0;\sigma_p\right)\left.\frac{\partial g_{0,j}^{(1)}}{\partial\xi}\right|_{H_0}&=D_p p^2\left(\xi,H_0;\sigma_p\right)\left.\frac{\partial^2 g_{0,j}^{(0)}}{\partial H_0^2}\right|_{\xi}\\&+\left[D_p+\nu_{f,p}p\left(\xi,H_0;\sigma_p\right)\right]\left.\frac{\partial g_{0,j}^{(0)}}{\partial H_0}\right|_{\xi}.\end{aligned} \tag{16}$$

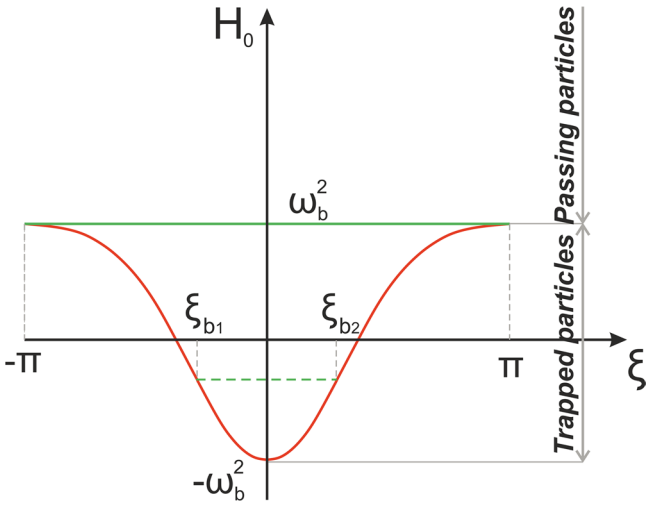

Figure 2. Sketch of H_0 against ξ at $p=0$. ξ varies from $-\pi$ to π outside the phase space island and between the bounce points, $\xi_{b1,2}$, given by $H_0=-\omega_b^2\cos\xi_{b1,2}$, inside the island region.

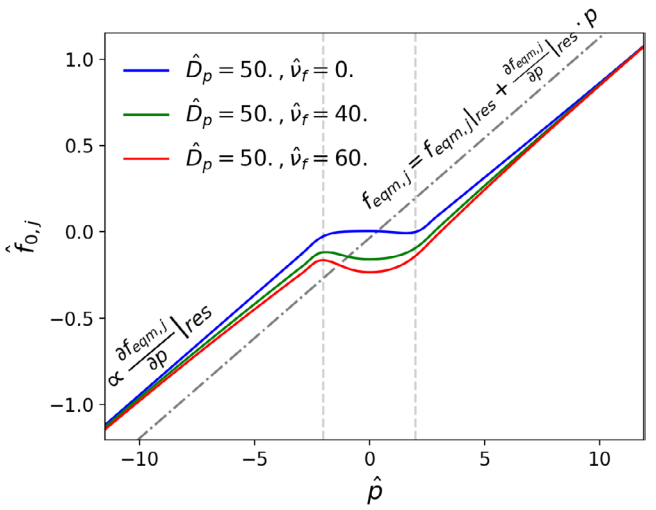

Figure 3. The EP distribution function $\hat{f}_{0,j}$ versus $\hat{p}$ across the island O-point, i.e. $\xi=0$, for arbitrary $\hat{D}_p$ and $\hat{\nu}_{f,p}$. The solution, $\hat{f}_{0,j}$, is localized to the island vicinity, which allows the initial equilibrium distribution function to be Taylor expanded in the vicinity of the resonant surface. Dashed lines indicate the position of the phase space island separatrix, $\hat{H}_0=\hat{\omega}_b^2$. Hats indicate the normalization that has been chosen as in [26].

To eliminate the term in $g_{0,j}^{(1)}$, we introduce an annihilation operator, which averages the free streaming term $\left.\frac{\partial g_{0,j}^{(1)}}{\partial\xi}\right|_{H_0}$ over ξ. For passing particles in phase space, i.e. particles outside the phase space island $H_0\geqslant\omega_b^2$ (see figure 2), we simply integrate over a period in ξ, requiring $g_{0,j}\left(-\pi\right)=g_{0,j}\left(\pi\right)$. For trapped particles inside the island, i.e. $-\omega_b^2\leqslant H_0<\omega_b^2$, we need to integrate equation (16) between the bounce points, given by $\xi_b=\pm\arccos\left(-H_0/\omega_b^2\right)$, and, in general, sum over the two streams, $\sigma_p=\pm1$, to provide continuity at each bounce point. Therefore, we introduce

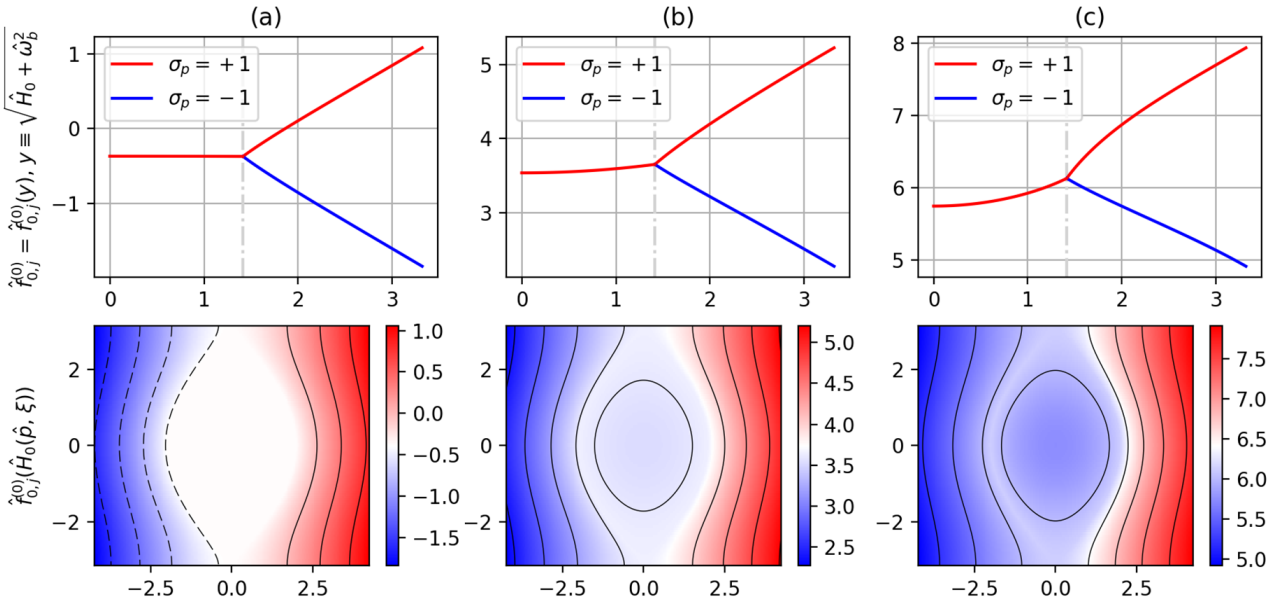

Figure 4. (top) The leading order EP distribution function as a function of $y = \sqrt{\hat{H}_0 + \hat{\omega}_b^2}$ for two branches of the stream, $\sigma_p = \pm 1$ for (*a*) a case of pure diffusion, (*b*) when velocity diffusion and drag are comparable and (*c*) when the drag term is dominant. The dotted line represents the trapped/passing boundary, $y_b = \sqrt{2}\hat{\omega}_b$. $y \geqslant y_b$ and $0 \leqslant y < y_b$ correspond to the passing and trapped regions, respectively. The trapped particle solution is σ_p-independent and hence both σ_p branches match in the trapped region. (bottom) Constant $\hat{f}^{(0)}_{0,j}$ contours in the $(\hat{p},\xi)$ plane, which repeat the phase space island structure; $\hat{\omega}_b = 1$. Hats indicate the normalization that has been chosen as in [26].

$$\langle ... \rangle_\xi = \begin{cases} \frac{1}{2\pi}\int_{-\pi}^{\pi} ...\mathrm{d}\xi, & H_0 \geqslant \omega_b^2 \\ \frac{1}{4\pi}\sum_{\sigma_p}\sigma_p \int_{-\xi_b}^{\xi_b} ...\mathrm{d}\xi, & -\omega_b^2 \leqslant H_0 < \omega_b^2 \end{cases} \quad (17)$$

ω_b^2 corresponds to the separatrix of the phase space island. Dividing both sides of equation (16) by $p(\xi, H_0; \sigma_p)$ and applying the ξ-averaging operator, equation (17), we arrive at the final equation for the leading order EP distribution function, $g^{(0)}_{0,j}$:

$$\langle D_p p(\xi, H_0; \sigma_p)\rangle_\xi \frac{\partial^2 g^{(0)}_{0,j}}{\partial H_0^2}\bigg|_\xi + \langle \frac{D_p}{p(\xi, H_0; \sigma_p)} + \nu_{f,p}\rangle_\xi \frac{\partial g^{(0)}_{0,j}}{\partial H_0}\bigg|_\xi = 0. \quad (18)$$

To match solutions at the trapped/passing boundary, $H_0^c = \omega_b^2$, we impose $\sum_{\sigma_p}\sigma_p g^p = 0$, $\sum_{\sigma_p} g^p = 2g^t$ and $\sum_{\sigma_p}\partial g^p/\partial H_0 = 2\partial g^t/\partial H_0$ to provide continuity across the boundary. Here indices p and t denote the passing and trapped regions, respectively. These matching conditions can be treated as the particle conservation law as we cross the boundary [27]. Far from the island, $f_{0,j}$ must be linear in p to match to the Maxwellian equilibrium distribution function (see figure 3). This linear behavior is provided by $f_{eqm,j}$ and as $f_{0,j} = f_{eqm,j} + g_{0,j}$, $g_{0,j}$ must satisfy $\partial_p g_{0,j}|_{p\to\pm\infty} = 0$. Solving this numerically for arbitrary D_p, $\nu_{f,p}$ and ω_b, we obtain $g^{(0)}_{0,j}$ as a function of H_0 for each σ_p. $f^{(0)}_{0,j}$ versus H_0 is shown in figure 4 for passing and trapped particles (the solution technique can be found in the appendix A.1). The solution in the trapped region has no σ_p dependence, which results from equation (17). Constant $f^{(0)}_{0,j}$ contours, plotted in figure 4 in the (p,ξ) plane, map out constant H_0 contours of the phase space islands. Once $f^{(0)}_{0,j} = f^{(0)}_{0,j}(H_0;\sigma_p)$ is found, we immediately obtain $f^{(0)}_{0,j}$ in p space, i.e. $f^{(0)}_{0,j}(H_0(\xi,p);\sigma_p)$.

The perturbative approach we apply breaks down in the 'dissipation' layer, i.e. in a narrow region of phase space in the vicinity of the island separatrix. Here collisional dissipation becomes comparable to free streaming $\sim p\partial/\partial\xi$, and a full solution of equation (14) is required. Solving equation (14) with similar boundary conditions in H_0 and applying $f_{0,j}(-\xi_b) = f_{0,j}(\xi_b)$ (ξ_b reduces to π for passing particles) in ξ, we obtain $f_{0,j} = f_{0,j}(\xi, H_0(\xi,p);\sigma_p)$. $f_{0,j}$ versus p is illustrated in figure 3 for arbitrary $\hat{D}_p$ and $\hat{\nu}_{f,p}$. As can be seen from the figure, in a pure diffusion case the flattening of the EP distribution function is maintained across the island. $f_{0,j}$ versus p approaches the Zakharov and Karpman solution [9], but with a more detailed treatment of the separatrix layer. Inclusion of drag modifies the distribution form significantly, creating a hole close to the island O-point, which grows with growing $\nu_{f,p}$. A similar destabilizing effect of dynamical friction was demonstrated by Lilley [24] in the slab geometry. Estimations, made in [24], show that the slowing down effect might be dominant over the collisional diffusion near the resonance region. As will be shown in section 4, a shape of the secondary mode Lagrangian and hence the corresponding dispersion function depend significantly on the amount of drag included.

In figures 5–7 we benchmark the EP distribution function, obtained as a solution of equation (14), against the full-f approach, provided by COBBLES (see appendix A.5 for more detail). Two scenarios are considered: (1) pure diffusion and (2) $\nu_{f,V} \gtrsim \nu_{d,V}$. The friction/diffusion ratio $\nu_{f,V}/\nu_{d,V} \lesssim 1$ in a typical NBI discharge and $\nu_{f,V}/\nu_{d,V} \gtrsim 1$ in the vicinity of the

TAE resonance ($\nu_{f,V}/\nu_{d,V} = 2.16$ chosen in our model). The behavior in the island region is found to be in good agreement with the COBBLES results. The discrepancy far from the island is expected and arises due to the difference in the boundary conditions we apply.

3.1. Self-consistency

We need to ensure that the perturbed Hamiltonian is consistent with the Maxwell set of equations. We restrict the analysis to the first harmonic of the distribution function in ξ, in accordance with the $\cos\xi$ form of the perturbed Hamiltonian. Hence, we define the following component $g^{\omega}_{0,j}$ of the distribution function:

$$g^{\omega}_{0,j}(J,t) = \oint \frac{\mathrm{d}\xi}{2\pi} g_{0,j}(\xi,J,t)\,\mathrm{e}^{-\mathrm{i}\xi}. \tag{19}$$

Maxwell's equations are equivalent to finding an extremum of the functional $\mathcal{L}(\omega) = \mathcal{L}^{(\mathrm{field})}(\omega) + \mathcal{L}^{(\mathrm{field})}(\omega)$ with respect to the vector potential $\boldsymbol{A}^*_{\omega}$ and electrostatic potential Φ^*_{ω}, where

$$\mathcal{L}^{(\mathrm{field})}(\omega) = \int \mathrm{d}\boldsymbol{x}\left(\varepsilon_0 \boldsymbol{E}_{\omega}\cdot\boldsymbol{E}^*_{\omega} - \frac{1}{\mu_0}\boldsymbol{B}_{\omega}\cdot\boldsymbol{B}^*_{\omega}\right) \tag{20}$$

and

$$\mathcal{L}^{(\mathrm{part})}(\omega) = \sum_j \int \mathrm{d}\boldsymbol{x}\,(\boldsymbol{j}_{\omega}\cdot\boldsymbol{A}^*_{\omega} - \rho_{\omega}\cdot\Phi^*_{\omega}). \tag{21}$$

Here $\boldsymbol{E}_{\omega}$ is the electric field, $\boldsymbol{B}_{\omega}$ the magnetic field, $\boldsymbol{j}_{\omega}$ the current density and ρ_{ω} the charge density. Summing over j represents a sum over all the species. A straightforward calculation shows that

$$\mathcal{L}^{(\mathrm{part})}(\omega) = -\sum_j \int \mathrm{d}\boldsymbol{x}\mathrm{d}\boldsymbol{p} g^{\omega}_{0,j} h^*_{\omega} - \sum_j \int \mathrm{d}\boldsymbol{x}\frac{n_j (eZ_j)^2}{m_j}\boldsymbol{A}_{\omega}\cdot\boldsymbol{A}^*_{\omega}, \tag{22}$$

where $h_{\omega} = eZ_j(\Phi_{\omega} - \boldsymbol{V}\cdot\boldsymbol{A}_{\omega})$ is the perturbed Hamiltonian, and $\boldsymbol{V} = (\boldsymbol{p} - eZ_j\boldsymbol{A}_{eqm}(\boldsymbol{x}))/m_j$ is the unperturbed velocity, which is a function of $(\boldsymbol{x},\boldsymbol{p})$. Solving a bump-on-tail problem, we drop the magnetic field contribution and reduce a problem to 2D in phase space. Hence, equations (20) and (22) are equivalent to equations (7) and (8). For $\delta\omega \ll \omega_0$ the Lagrangian can be written as $\mathcal{L}(\omega) = \mathcal{L}_0(\omega) + \mathcal{L}_1(\omega)$. Here $\mathcal{L}_0$ is real and is related to the magnetohydrodynamic (MHD) energy, δW_{MHD}, (it can be shown that $\mathcal{L}_0 = -2\delta W_{\mathrm{MHD}}$) and $\mathcal{L}_1$ represents the weak resonant interaction between the perturbed electro-magnetic field and particles. Hence for one resonant species, $\mathcal{L}_1 = \int \mathrm{d}\boldsymbol{x}\mathrm{d}\boldsymbol{p} g^{\omega}_{0,j} h^*_{\omega}$. The functional $\mathcal{L}_1$ is complex, in particular $2\omega\Im\mathcal{L}_1$ measures the resonant energy exchange between the mode and the exciting particles. At lowest order, we find a dispersion relation that gives the reference real pulsation, ω_0, i.e. $\mathcal{L}_0(\omega_0) = 0$. The first order reads

$$2\omega_0 \left.\frac{\partial\mathcal{L}_0}{\partial\omega}\right|_{\omega=\omega_0} [\delta\omega + \mathrm{i}(\gamma+\gamma_d)] = -2\omega_0\mathcal{L}_1. \tag{23}$$

Setting $\Lambda_{\omega} = \omega_0\,\partial\mathcal{L}_0/\partial\omega|_{\omega=\omega_0}$ (mode energy frequency), we find the following constraint

$$\begin{aligned}\delta\omega &= -\frac{\omega_0}{\Lambda_{\omega}}\Re\mathcal{L}_1,\\ \gamma &= -\frac{\omega_0}{\Lambda_{\omega}}\Im\mathcal{L}_1 - \gamma_d.\end{aligned} \tag{24}$$

The first equation in equation (24) is a correction to the dispersion relation that provides the frequency shift, $\delta\omega$, while the second one is an energy balance equation, which provides the growth/decay rate of the wave, γ. Here an ad-hoc damping rate, γ_d, has been added to equation (24). When a second stabilizing species is added, it corresponds to an energy sink due to the Landau damping. Rewriting the phase space element in terms of ξ, $\mathcal{L}_1 = \frac{2h^2_{\omega}}{\omega^2_b}\int_{-\pi}^{\pi}\frac{\mathrm{d}\xi}{2\pi}\mathrm{d}p g_{0,j}(\xi,p,t)\,\mathrm{e}^{-\mathrm{i}\xi}$, where $\frac{\mathrm{d}\xi}{2\pi}\mathrm{d}p = \sum_{\sigma_p}\frac{\mathrm{d}\xi}{2\pi}\frac{\mathrm{d}H_0}{p} = \sum_{\sigma_p}\frac{\mathrm{d}\xi}{2\pi}\frac{\mathrm{d}J}{\tau p}$. Then equation (24) becomes

$$\begin{aligned}\delta\omega &= -2\frac{\omega_0}{\omega^2_b}\frac{h^2_{\omega}}{\Lambda_{\omega}}\sum_{\sigma_p}\int_0^{J_{\max}}\mathrm{d}J\langle g_{0,j}\cos\xi\rangle_{\xi},\\ \gamma &= 2\frac{\omega_0}{\omega^2_b}\frac{h^2_{\omega}}{\Lambda_{\omega}}\sum_{\sigma_p}\int_0^{J_{\max}}\mathrm{d}J\langle g_{0,j}\sin\xi\rangle_{\xi} - \gamma_d,\end{aligned} \tag{25}$$

where $J_{\max}$ is chosen so that the integration domain covers the whole phase space, inside and outside the island, i.e. $J_{\max} = \infty$, which is also valid for the Zakharov–Karpman solution [9]. To provide a link to the Berk and Breizman case, we choose $J_{\max}$ corresponding to the separatrix of a hole or a clump and replace $g_{0,j}$, defined as $f_{0,j} - f_{eqm,j}$, by $f_{0,j} - f_{eqm,j}|_{\mathrm{res}} - (\partial f_{eqm,j}/\partial p)|_{\mathrm{res}}p$ (here *res* denotes the resonant surface), since $J = 0$ corresponds to the hole/clump center. In the Berk–Breizman conventions, there is no sum over σ_p in equation (25), as the action, J, encompasses both branches of the bounce motion. Setting $\gamma_L = \pi\omega_0\left.\frac{\partial f_{eqm,j}}{\partial p}\right|_{\mathrm{res}}\frac{h^2_{\omega}}{\Lambda_{\omega}}$ as in [1, 2], we recover the main result of [1, 2]:

$$\begin{pmatrix}-\delta\omega\\ \gamma_d\end{pmatrix} = \frac{2}{\pi}\frac{\gamma_L}{\omega^2_b}\left(\left.\frac{\partial f_{eqm,j}}{\partial p}\right|_{\mathrm{res}}\right)^{-1}\sum_{\sigma_p}\int_0^{J_{\max}}\mathrm{d}J\begin{pmatrix}\langle g_{0,j}\cos\xi\rangle_{\xi}\\ \langle g_{0,j}\sin\xi\rangle_{\xi}\end{pmatrix}. \tag{26}$$

Here γ has been taken as zero, i.e. no exponential growth/decay is assumed. Note that γ_L does not depend on the amplitude since the mode energy density Λ_{ω} scales as h^2_{ω}. It is easy to verify that γ_L is the linear growth rate in the absence of dissipation, i.e. $\gamma_d = 0$. Indeed, the linear solution of the Vlasov equation is $g_{0,j} = -\frac{1}{2}\left.\frac{\partial f_{eqm,j}}{\partial p}\right|_{\mathrm{res}}\frac{\omega^2_b}{p-\mathrm{i}0^+}$, so that $\Im\mathcal{L}_1 = \frac{2h^2_{\omega}}{\omega^2_b}\int_{\mathbb{R}}\mathrm{d}p\Im g_{0,j} = -\pi h^2_{\omega}\left.\frac{\partial f_{eqm,j}}{\partial p}\right|_{\mathrm{res}}$. Substituting this into equation (24) yields the growth rate $\gamma = \gamma_L - \gamma_d$, where γ_L is defined above. It appears that $\gamma = \gamma_L$ when $\gamma_d = 0$, so that γ_L can be interpreted as a linear growth rate in the absence of dissipation.

4. Stability analysis. Secondary modes

4.1. Filtered solution

If $f_{0,j}$ has no ξ-dependence, either because $p \gg \omega_b$ (thermal particles) or $f_{0,j}$ is averaged over ξ (filtered solution), the solution of equation (9) is simply

$$f_{j,k\omega} = -\frac{l}{\delta\omega - lp + \mathrm{i}0^+}\left\langle\frac{\partial f_{0,j}}{\partial p}\right\rangle_\xi h_{k\omega}. \tag{27}$$

Using equations (7) and (8), we obtain

$$\mathcal{L}(\delta\omega, l) = \left[-l^2 - \sum_j \omega_{pj}^2 \int_{\mathbb{R}} \frac{l}{\delta\omega - lp + \mathrm{i}0^+}\left\langle\frac{\partial f_{0,j}}{\partial p}\right\rangle_\xi \mathrm{d}p\right] |h_{k\omega}|^2. \tag{28}$$

For thermal background, $f_{0,j}$ is given by a non-shifted Maxwellian, $f_j^M = \frac{1}{(2\pi)^{1/2}V_{Tj}}\mathrm{e}^{-V^2/2V_{Tj}^2}$ with $V_{Tj} = \sqrt{T_j/m_j}$ being the thermal velocity. Hence, the dispersion relation $\mathcal{L}(\delta\omega, l) = 0$ for the background electrons and ions reads $1 - \sum_{j=e,i}\frac{\omega_{pj}^2}{\omega_{tj}^2}\int_{\mathbb{R}}\frac{\mathrm{d}\varsigma}{(2\pi)^{1/2}}\mathrm{e}^{-\varsigma^2/2}\frac{\omega_{tj}\varsigma}{\omega - \omega_{tj}\varsigma + \mathrm{i}0^+} = 0$, where $\omega_{tj} = kV_{Tj}$ is the transit frequency. For a mode close to marginality $\gamma = \Im\omega \ll \omega_r = \Re\omega$, and in the large frequency limit $\omega \sim \omega_{pj} \gg \omega_{tj}$, we can apply the Sokhotski–Plemelj formula to obtain approximately $\frac{1}{\omega - \omega_{tj}\varsigma + \mathrm{i}0^+} \simeq \frac{1}{\omega}\left(1 + \frac{\omega_{tj}\varsigma}{\omega}\right) - \mathrm{i}\pi\delta(\omega - \omega_{tj}\varsigma)$, where δ denotes the Dirac delta function. Hence, an approximate dispersion relation becomes $1 - \sum_{j=e,i}\left[\frac{\omega_{pj}^2}{\omega^2} - \mathrm{i}\left(\frac{\pi}{2}\right)^{1/2}\frac{\omega\omega_{pj}^2}{\omega_{tj}^3}\mathrm{e}^{-\omega_{pj}^2/2\omega_{tj}^2}\right] = 0$. Expanding this with respect to $\gamma/\omega_r \ll 1$, we find $\omega_r \simeq \omega_{pe}$ and $\gamma = -\gamma_e$, $\gamma_e = \frac{1}{2}\left(\frac{\pi}{2}\right)^{1/2}\omega_{pe}\frac{\omega_{pe}^3}{\omega_{te}^3}\mathrm{e}^{-\omega_{pe}^2/2\omega_{te}^2}$, where we have used the fact that $\omega_{pe} \gg \omega_{pi}$. This is the conventional expression for the Landau damping rate of the Langmuir wave. Thus, the functional for thermal particles can be approximated by

$$\mathcal{L}_j(\delta\omega, l) = l^2\left(\frac{\omega_{pj}^2}{\omega^2} + 2\mathrm{i}\frac{\omega\gamma_j}{\omega_{pj}^2}\right)|h_{k\omega}|^2. \tag{29}$$

$j = e, i$ here indicates main electrons/ions. In the absence of thermal particles, this term vanishes. The fast particle contribution is then

$$\mathcal{L}_{\mathrm{EP},j}(\delta\omega, l) = -\omega_{pj}^2\left[\int_{\mathbb{R}}\frac{l}{\delta\omega - lp + \mathrm{i}0^+}\left\langle\frac{\partial f_{0,j}}{\partial p}\right\rangle_\xi \mathrm{d}p\right]|h_{k\omega}|^2. \tag{30}$$

In equation (30) $j = \mathrm{fe}, \mathrm{fi}$ indicates fast electrons/ions that drive the bump-on-tail instability. The total Lagrangian, given by equation (7), has the form $L(\delta\omega, l) = D(\delta\omega, l)|h_{k\omega}|^2$, where D is the dispersion function. Hence, the dispersion relation reads

$$-1 + \sum_{j=e,i}\left(\frac{\omega_{pj}^2}{\omega^2} + 2\mathrm{i}\frac{\omega\gamma_j}{\omega_{pj}^2}\right) - \sum_{j=\mathrm{fe,fi}}\frac{\omega_{pj}^2}{l^2}\int_{\mathbb{R}}\frac{l}{\delta\omega - lp + \mathrm{i}0^+}\left\langle\frac{\partial f_{0,j}}{\partial p}\right\rangle_\xi \mathrm{d}p = 0. \tag{31}$$

4.2. Full solution of the Vlasov/Fokker–Planck—Poisson system

4.2.1. Formal solution of the Vlasov/Fokker–Planck equation. Let us start with the perturbed Vlasov/Fokker–Planck equation, equation (9), which we rewrite as

$$-\mathrm{i}\delta\omega f_{j\omega} + p\frac{\partial f_{j\omega}}{\partial\xi} = \mathrm{i}lp\frac{\partial f_{0,j}}{\partial H_0}h_{k\omega}\mathrm{e}^{\mathrm{i}l\xi}, \tag{32}$$

where $f_{j\omega}$ and p are now functions of ξ, H_0 and σ_p, while $h_{k\omega}$ is assumed to be a constant. $f_{0,j}$ is the primary equilibrium distribution function, found in the previous section for the EP component (and assumed to be Maxwellian for the electron/ion background). To simplify the analysis, we split the distribution function into an adiabatic response and a resonant part, i.e.

$$f_{j\omega} = \frac{\partial f_{0,j}}{\partial H_0}h_{k\omega}\mathrm{e}^{\mathrm{i}l\xi} + g_{j\omega}, \tag{33}$$

respectively. Solving equation (32) for $g_{j\omega}$, we find

$$g_{j\omega} = \mathrm{i}\delta\omega\frac{\partial f_{0,j}}{\partial H_0}h_{k\omega}\mathrm{e}^{\mathrm{i}\delta\omega Q}\left[\int_{-\xi_b}^{\xi}\frac{\mathrm{d}\xi'}{p'}\mathrm{e}^{\mathrm{i}l\xi' - \mathrm{i}\delta\omega Q'} + C(\sigma_p)\right], \tag{34}$$

where p' and Q' are abbreviations for $p(\xi', H_0; \sigma_p)$ and $Q(\xi', H_0; \sigma_p)$ (note that ξ_b becomes π for the passing branch). Q is defined as

$$Q(\xi, H_0; \sigma_p) = \int_0^\xi \frac{\mathrm{d}\xi'}{p(\xi', H_0; \sigma_p)}, \tag{35}$$

which has an equivalent representation through the incomplete elliptic integral of the first kind, $\sqrt{2}\sigma_p\left(H_0 + \omega_b^2\right)^{-1/2}F\left(\frac{\xi}{2}, \frac{2\omega_b^2}{H_0 + \omega_b^2}\right)$. $C(\sigma_p)$ is a constant of integration that is different on each branch of σ_p and is to be determined in next section. The EP Lagrangian is then

$$\mathcal{L}_{\mathrm{EP},j}(\delta\omega, l) = \omega_{pj}^2\sum_{\sigma_p}\int_{-\omega_b^2}^{+\infty}\mathrm{d}H_0\oint\frac{\mathrm{d}\xi}{2\pi}\frac{1}{p}f_{j\omega}h_{k\omega}^*\mathrm{e}^{-\mathrm{i}l\xi}, \tag{36}$$

where we have used $\int_{\mathbb{R}}\mathrm{d}p\int_{-\pi}^{\pi}\frac{\mathrm{d}\xi}{2\pi} = \sum_{\sigma_p}\int_{-\omega_b^2}^{+\infty}\mathrm{d}H_0\oint\frac{\mathrm{d}\xi}{2\pi}\frac{1}{p}$. Equation (36) can be split into the adiabatic and resonant parts, $\mathcal{L}_{\mathrm{EP},j}(\delta\omega, l) = \mathcal{L}_{ad,j}(\delta\omega, l) + \mathcal{L}_{\mathrm{res},j}(\delta\omega, l)$, by substituting equation (33). It can be shown that the energy exchange between waves and particles is given by the imaginary part of $\mathcal{L}_{\mathrm{EP},j}(\delta\omega, l)$. Hence, the adiabatic response does not contribute to the exchange of energy, only $\mathcal{L}_{\mathrm{res},j}$ does. At this stage, $C(\sigma_p)$ remains to be calculated.

4.2.2. Matching conditions. In the previous section we have determined the perturbed distribution function, $g_{j\omega}$, in terms of the arbitrary constant, $C(\sigma_p)$. In this section we introduce an angle variable α to determine C, and hence to derive the full EP distribution.

To calculate C, we need to maintain the matching procedure. Let us introduce $-\xi_0$ as a starting point in ξ. For passing particles the distribution function must have the same value at $\xi = -\xi_0$ and $\xi = \xi_0$ for each sign of p. This can be easily provided. However, the trapped particle distribution function must be matched both, at $\xi = \xi_0$ after half a bounce on the interval $[-\xi_0; \xi_0]$ and again at $\xi = -\xi_0$ at the end of the way back to the initial bounce angle. Note that when a particle moves from $-\xi_0$ to ξ_0, it has a positive momentum p, while p is negative on the return branch, from ξ_0 to $-\xi_0$. So both branches, $\sigma_p = \pm 1$, are connected at constant energy H_0. To simplify the $C(\sigma_p)$ calculation, we introduce the following variable α instead of ξ for trapped particles:

$$\alpha = \Omega_b \int_0^{\xi} \frac{\mathrm{d}\xi'}{p'}, \quad p > 0 \tag{37}$$

and

$$\alpha = \pi - \Omega_b \int_0^{\xi} \frac{\mathrm{d}\xi'}{p'}, \quad p < 0 \tag{38}$$

with $\Omega_b(H_0) = \left(\int_{-\xi_0}^{\xi_0} \frac{\mathrm{d}\xi}{\pi|p|}\right)^{-1}$ being the bounce frequency (ω_b is its limit value at the deeply trapped end, i.e. $H_0 \to -\omega_b^2$). Here we note

- α increases monotonically with ξ along the trapped trajectory at given H_0. It varies from $-\pi/2$ to $\pi/2$ for $\xi \in [-\xi_0; \xi_0]$, and from $\pi/2$ to $3\pi/2$ on the way back, i.e. $\xi \in [\xi_0; -\xi_0]$.
- α is an angle variable since it spans $[-\pi/2; 3\pi/2]$ along the closed trapped trajectory.
- the choice grants that $\xi = \xi(H_0, \alpha)$ is an odd function of α. It also satisfies $\xi(H_0, \alpha; \sigma_p = +1) = \xi(H_0, \pi - \alpha; \sigma_p = -1)$. Hence, the relation between α and ξ, given above, can be inverted. Therefore, we find it convenient to express $g_{j\omega}$ as a function of H_0 and α only; α also contains the information on σ_p. According to Barrow's theorem, we have $\mathrm{d}\alpha/\Omega_b = \mathrm{d}\xi/p$ for both branches. The exact same expression is valid for passing particles, as we will see later in this section.
- This procedure guarantees that if $g_{j\omega}$ is treated as a function of α instead of ξ, it is continuous at $\xi = \xi_0$, i.e. $\alpha = \pi/2$, which leaves the only one constant C to determine for trapped particles.

$g_{j\omega}$ then takes the form:

$$g_{j\omega} = \mathrm{i}\delta\omega \frac{\partial f_{0,j}}{\partial H_0} h_{k\omega} \mathrm{e}^{\mathrm{i}\frac{\delta\omega}{\Omega_b}\alpha} \left[\int_{-\pi/2}^{\alpha} \frac{\mathrm{d}\alpha'}{\Omega_b} \mathrm{e}^{\mathrm{i}\left(l\xi' - \frac{\delta\omega}{\Omega_b}\alpha'\right)} + C(\sigma_p)\right], \tag{39}$$

valid for $-\pi/2 \leqslant \alpha < 3\pi/2$. We still have to provide its continuity at $\xi = -\xi_0$ after one bounce, i.e. $g_{j\omega}(H_0, \alpha = -\pi/2) = g_{j\omega}(H_0, \alpha = 3\pi/2)$, which gives immediately

$$C = \frac{\int_{-\pi}^{\pi} \frac{\mathrm{d}\alpha}{\Omega_b} \mathrm{e}^{\mathrm{i}\left(l\xi - \frac{\delta\omega}{\Omega_b}\alpha\right)}}{\mathrm{e}^{-2\pi\mathrm{i}\frac{\delta\omega}{\Omega_b}} - 1}. \tag{40}$$

Here we have used the fact that limits of integration can be shifted for a periodic function, integrated over the length of the period (note that periodicity in α is provided by the choice of α, while periodicity in ξ is not required). An equivalent expression for C can be obtained by the relation

$$\sum_{k=1}^{+\infty} \mathrm{e}^{2\pi k\mathrm{i}\frac{\delta\omega}{\Omega_b}} = \frac{1}{\mathrm{e}^{-2\pi\mathrm{i}\frac{\delta\omega}{\Omega_b}} - 1} \tag{41}$$

(see appendix A.2 for more detail). Rewriting the resonant part of the EP Lagrangian in terms of α, we obtain

$$\mathcal{L}_{\mathrm{res},j}(\delta\omega, l) = 2\pi\mathrm{i}\delta\omega \cdot \omega_{pj}^2 |h_{k\omega}|^2 \int_{-\omega_b^2}^{+\infty} \frac{\mathrm{d}H_0}{\Omega_b^2} \int_{-\pi}^{\pi} \frac{\mathrm{d}\alpha}{2\pi} \frac{\partial f_{0,j}}{\partial H_0} \mathrm{e}^{-\mathrm{i}\left(l\xi - \frac{\delta\omega}{\Omega_b}\alpha\right)} \left[\int_{-\pi/2}^{\alpha} \frac{\mathrm{d}\alpha'}{2\pi} \mathrm{e}^{\mathrm{i}\left(l\xi' - \frac{\delta\omega}{\Omega_b}\alpha'\right)} + C(\sigma_p)\right] \tag{42}$$

for trapped particles (with $C(\sigma_p)$ given by equation (40)). Here both, α and α' have been shifted by $\pi/2$ for convenience. Note that α' can be introduced as an extended angle that spans the interval $(-\infty; \pi]$ and hence an integral over $\alpha' \in [-\pi/2, \alpha]$ can be replaced by $\alpha' \in (-\infty; \alpha]$.

To consider passing particles, we note that branches $\sigma_p = \pm 1$ are no longer connected. Nevertheless, we still can introduce a similar change of variables:

$$\alpha = \Omega_b \int_0^{\xi} \frac{\mathrm{d}\xi'}{p'} \tag{43}$$

with $\Omega_b(H_0) = \sigma_p \left(\int_{-\pi}^{\pi} \frac{\mathrm{d}\xi}{2\pi|p|}\right)^{-1}$ being the transit frequency. The properties of $\alpha(\xi, H_0; \sigma_p)$ for passing particles are the same as described above for trapped particles. We note that the bounce frequency, Ω_b, is negative when $\sigma_p = -1$, and hence ξ and α rotate in opposite directions. Thus, we arrive at the final expression for the resonant Lagrangian of the form:

$$\mathcal{L}_{\mathrm{res},j}(\delta\omega, l) = 2\pi\mathrm{i}\omega_{pj}^2 |h_{k\omega}|^2 \sum_{\sigma_p} \int_{-\omega_b^2}^{+\infty} \frac{\mathrm{d}H_0}{\Omega_b} \frac{\delta\omega}{|\Omega_b|} \int_{-\pi}^{\pi} \frac{\mathrm{d}\alpha}{2\pi} \frac{\partial f_{0,j}}{\partial H_0} \mathrm{e}^{-\mathrm{i}\left(l\xi - \frac{\delta\omega}{\Omega_b}\alpha\right)} \left[\int_{-\infty}^{+\infty} \frac{\mathrm{d}\alpha'}{2\pi} \mathrm{e}^{\mathrm{i}\left(l\xi' - \frac{\delta\omega}{\Omega_b}\alpha'\right)} \cdot \Theta[\sigma_p(\alpha - \alpha')] + C(\sigma_p)\right], \tag{44}$$

where Θ is the Heaviside step function. The summation over σ_p applies only to the passing domain with σ_p being the sign of Ω_b. This convention will be used throughout the paper, unless otherwise stated. To check the validity of equation (44), we address the limit when the trapped particle contribution becomes negligible, and ξ can be considered as a linear function of α, i.e. the limit of deeply passing particles. Then we recover the solution for thermal particles, found in equation (28), and the dispersion relation of the bump-on-tail instability in accordance with equation (31).

4.2.3. Explicit resonance form. To establish a connection with the filtered solution, we seek an expression for equation (44), where resonances are explicit. This representation must be valid everywhere in phase space, as we would expect to see secondary modes in a region with the largest gradient of the primary equilibrium distribution function, $f_{0,j}(H_0)$. From a technical point of view, we need to re-express equation (34)/ equation (39) and hence the functional equation (44) in a resonant form. This is tricky, but the calculation becomes straightforward with the following remark: since the new variable α is an angle for both trapped and passing particles, we can seek $g_{j\omega}$ as a Fourier series in α, i.e.

$$g_{j\omega}(\alpha, H_0; \sigma_p) = \sum_n g_{j,n\omega}(H_0; \sigma_p) \mathrm{e}^{\mathrm{i}n\alpha}. \tag{45}$$

Here the σ_p dependence is relevant to passing particles only. Since the perturbed Hamiltonian is an exponential function of ξ, it is also an exponential function of α, but with an infinite number of harmonics instead of only one harmonic in ξ:

$$h_\omega = h_{k\omega} e^{il\xi} = \sum_{n=-\infty}^{+\infty} h_{n\omega}(H_0;\sigma_p)\, e^{in\alpha}. \tag{46}$$

Using $d\alpha/\Omega_b = d\xi/p$, we come to the following solution of the Vlasov/Fokker–Planck equation:

$$g_{j,n\omega} = -\frac{\delta\omega}{\delta\omega - n\Omega_b + i0^+}\frac{\partial f_{0,j}}{\partial H_0} h_{n\omega} \tag{47}$$

and the corresponding resonant Lagrangian:

$$\mathcal{L}_{\mathrm{res},j}(\delta\omega, l) = -\omega_{pj}^2 \sum_{n=-\infty}^{+\infty}\sum_{\sigma_p}\int_{-\omega_b^2}^{+\infty} \frac{dH_0}{\Omega_b}\frac{\delta\omega}{\delta\omega - n\Omega_b + i0^+}\frac{\partial f_{0,j}}{\partial H_0}|h_{n\omega}|^2, \tag{48}$$

where the perturbed Hamiltonian Fourier components, $h_{n\omega}$, are

$$h_{n\omega} = h_{k\omega}\int_{-\pi}^{\pi}\frac{d\alpha}{2\pi} e^{i(l\xi - n\alpha)}. \tag{49}$$

ξ here is a function of $(\alpha, H_0; \sigma_p)$. We note that n differs from l, except for the deeply passing end, $H_0 \to +\infty$, since $\alpha = \xi$ in that case. It can be proved that equations (44), (48) and (49) are equivalent (see appendix A.2 for more detail). Adding the adiabatic contribution, we have

$$\mathcal{L}_{\mathrm{EP},j}(\delta\omega, l) = -\omega_{pj}^2 \sum_{n=-\infty}^{+\infty}\sum_{\sigma_p}\int_{-\omega_b^2}^{+\infty} \frac{dH_0}{\Omega_b}\frac{n\Omega_b}{\delta\omega - n\Omega_b + i0^+}\frac{\partial f_{0,j}}{\partial H_0}|h_{n\omega}|^2 \tag{50}$$

for the total EP Lagrangian. Equation (50) has a form close to the filtered dispersion relation but still is an exact solution of the problem.

4.2.4. Full secondary mode dispersion relation. When the island-like structure is fully accounted for, the dispersion function takes two forms. The resonant form is

$$D(\delta\omega, l) = -l^2 + l^2\sum_{j=e,i}\left(\frac{\omega_{pj}^2}{\omega^2} + 2i\frac{\omega\gamma_j}{\omega_{pj}^2}\right) - \sum_{j=\mathrm{fe,fi}}\omega_{pj}^2\sum_{n=-\infty}^{+\infty}\sum_{\sigma_p}\int_{-\omega_b^2}^{+\infty}\frac{dH_0}{\Omega_b}\frac{n\Omega_b}{\delta\omega - n\Omega_b + i0^+}\frac{\partial f_{0,j}}{\partial H_0}\left|\bar{h}_{n\omega}\right|^2 \tag{51}$$

with the coefficients $\bar{h}_{n\omega}$ defined as

$$\bar{h}_{n\omega} = \int_{-\pi}^{\pi}\frac{d\alpha}{2\pi} e^{i(l\xi - n\alpha)}. \tag{52}$$

An equivalent non-resonant form reads

$$D(\delta\omega, l) = -l^2 + l^2\sum_{j=e,i}\left(\frac{\omega_{pj}^2}{\omega^2} + 2i\frac{\omega\gamma_j}{\omega_{pj}^2}\right) + \sum_{j=\mathrm{fe,fi}}\omega_{pj}^2\sum_{\sigma_p}\int_{-\omega_b^2}^{+\infty}\frac{dH_0}{\Omega_b}\frac{\partial f_{0,j}}{\partial H_0} + 2\pi i\sum_{j=\mathrm{fe,fi}}\omega_{pj}^2\sum_{\sigma_p}\int_{-\omega_b^2}^{+\infty}\frac{dH_0}{\Omega_b}\frac{\delta\omega}{|\Omega_b|}\frac{\partial f_{0,j}}{\partial H_0}\int_{-\pi}^{\pi}\frac{d\alpha}{2\pi}e^{-i\left(l\xi - \frac{\delta\omega}{\Omega_b}\alpha\right)} \times\left\{\int_{-\infty}^{+\infty}\frac{d\alpha'}{2\pi}e^{i\left(l\xi' - \frac{\delta\omega}{\Omega_b}\alpha'\right)}\cdot\Theta[\sigma_p(\alpha - \alpha')] + C(\sigma_p)\right\} \tag{53}$$

(note: equations (51) and (52)/equation (53) reduces to the conventional bump-on-tail dispersion relation, equation (31), in the limit of deeply passing particles, i.e. $H_0 \gg \omega_b^2$.) Here $\delta\omega$ is complex and takes the form $\delta\omega + i\gamma$. γ corresponds to the secondary mode growth/decay rate. $D(\delta\omega, \gamma) = 0$ provides the secondary mode dispersion relation. To analyze its stability, we consider contours of constant $|D(\delta\omega, \gamma)|$ in the $(\delta\omega, \gamma)$ plane [26]. Any root of $|D(\delta\omega, \gamma)|$ corresponds to a pole of $|D(\delta\omega, \gamma)|^{-1}$. For simplicity, we focus on fast electrons, dropping the background ion term in the dispersion function, as $\omega_{pi} \ll \omega_{pe}$, provided the plasma quasineutrality is maintained. The fraction of EPs is assumed to be small by default. In [26] we have investigated the D_p, $\nu_{f,p}$ and l dependencies of the secondary mode growth/decay rate. γ as a function of the velocity diffusion and dynamical friction rates has been found to be monotonic, and changing the sign of γ in a chosen range of plasma and wave parameters. In contrast, γ versus l, found in [26], has two roots, which provide the secondary mode stability regions. In figure 8 we plot the secondary mode growth/decay rate, γ, against $l = k/k_0$, based on the full secondary mode dispersion relation, equations (51) and (52)/equation (53), with $f_{0,j}$ found as a solution of equation (14) and shown in figure 5. As can be seen from the figure, the secondary mode is stable for $l < l_c$ and $l \geqslant l_s$. l_c and l_s are introduced as roots of $\gamma = \gamma(l)$ and hence define the stability region(s) of secondary modes. l_c has been shown to grow monotonically with the dynamical friction rate [26] in a chosen range of plasma and wave parameters. However, this variation of l_c with $\nu_{f,p}$ is weak in both figure 3 of [26] and figure 8 to change the stability region(s) significantly. Due to a larger number of poles of $|D|^{-1}$ in the decreasing region of γ versus l, we introduce two decreasing branches. This gives two maximum values of γ as a function l. Indeed, provided ω_0/k_0 and ω/k are the primary island and the secondary mode resonant velocities, we estimate a value of l that corresponds to the maximum growth rate of the secondary modes from $\omega/k \approx \omega_0/k_0 \pm 2\omega_b/k_0$. The maximum growth rate is expected when the secondary mode resonant velocity approaches the boundary of the primary island, $\pm 2\omega_b/k_0$. This can be explained by steepening of the particle distribution in the vicinity of the island separatrix due to its flattening in the island region in a pure diffusion case as well as its hole close to the island O-point in the presence of drag (see figures 5–7 for the primary equilibrium distribution). As $\omega \approx \omega_0 \approx \omega_{pe}$ to leading order, the latter condition roughly translates into $1 \pm 2\omega_b/\omega_{pe} \approx k_0/k = 1/l$, which provides an estimation for l for a given island half-width, ω_b (0.83 and 1.25 for $\omega_b = 0.1$, respectively). As can be seen from figure 8, γ as a function of l is non-monotonic with maximums being in accordance with these estimations. Adding drag creates a hole at the O-point of the island and hence shifts the largest gradient of the EP distribution closer to the island center, which, in turn, decreases the stationary point of $\gamma = \gamma(l)$.

The other parameter we can vary is the bounce frequency of deeply trapped particles that characterizes the width of the island in phase space, $2\omega_b$. We plot γ against ω_b for different friction rates (figure 9) and in a pure diffusion case for different

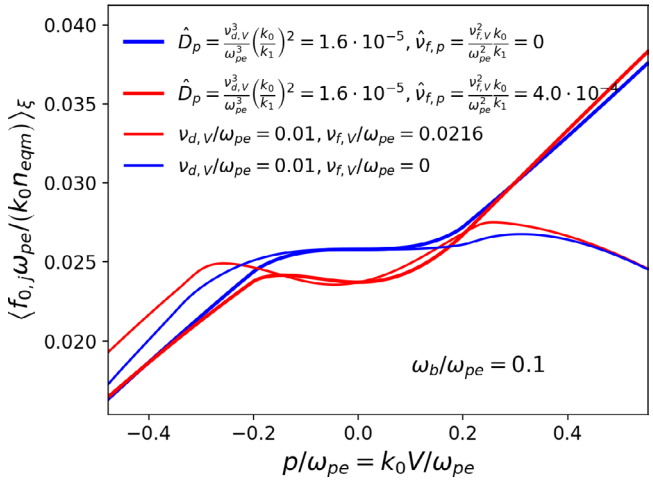

Figure 5. The ξ-averaged EP distribution function, $\langle f_{0,j}\rangle_\xi$, versus p for arbitrary D_p and $\nu_{f,p}$, $\omega_b = 0.1\omega_{pe}$. $f_{0,j}$ is normalized to $n_{eqm}k_0/\omega_{pe}$, n_{eqm} is the equilibrium density. Thick lines indicate the solution of equation (14), which is localized to the island vicinity. Thin lines indicate the COBBLES distribution function. Diffusion and friction rates in velocity space are $\nu_{d,V} = 0.01\omega_{pe}$ and $\nu_{f,V} = 0$ (blue curves), $\nu_{d,V} = 0.01\omega_{pe}$ and $\nu_{f,V} = 0.0216\omega_{pe}$ (red curves). In p space, these correspond to diffusion $D_p = \nu_{d,V}^3(k_0/k_1)^2 = 1.6\cdot10^{-5}\omega_{pe}^3$ and drag $\nu_{f,p} = \nu_{f,V}^2(k_0/k_1) = 0/4.0\cdot10^{-4}\omega_{pe}^2$, respectively. $\nu_{f,V}/\nu_{d,V} = 2.16$.

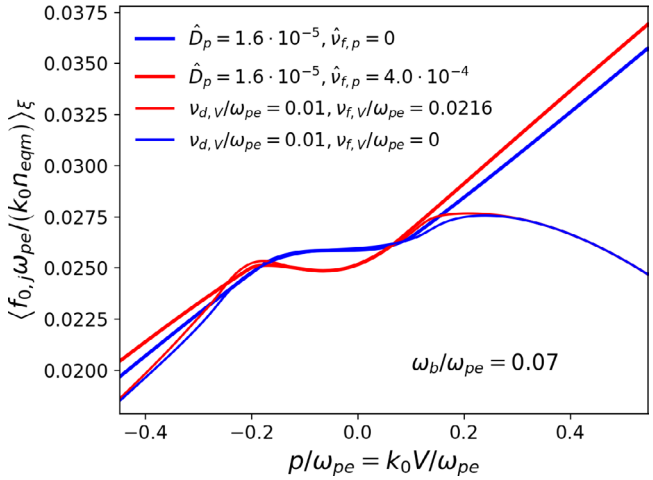

Figure 6. Same as figure 5 except for the bounce frequency value, $\omega_b = 0.07\omega_{pe}$.

bulk densities (figure 10). This functional dependence is non-monotonic and provides a region of marginal stability of secondary modes. γ grows monotonically with ω_b, crossing the $\gamma = 0$ level. Then it reaches maximum and decreases, crossing $\gamma = 0$ for the second time. Hence, we introduce a marginal island half-width, $\omega_{b,c}$, below which $\gamma < 0$ and thus the mode is stable, as well as a saturation level, $\omega_{b,s}$, where γ as a function of ω_b has a second root.

The solution has been benchmarked against the full-f approach. In figure 10 we plot the secondary mode growth/decay rate versus ω_b for different equilibrium plasma density, n_e, and the ad-hoc damping rate, $\gamma_{d,0}$. An analytic solution is governed by equations (51) and (52)/equation (53), while the

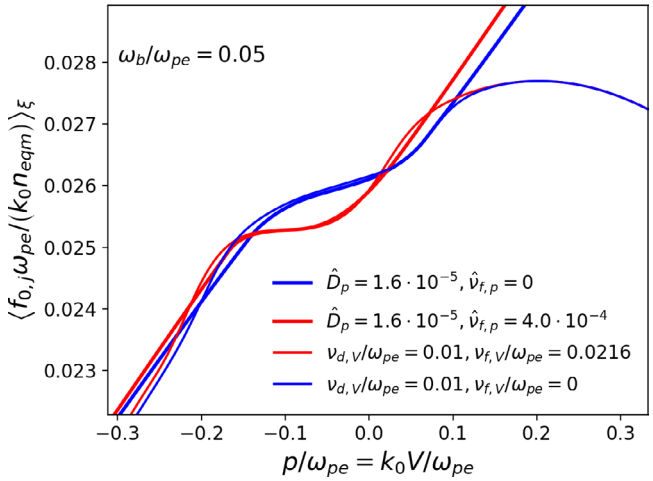

Figure 7. Same as figure 5 except for the bounce frequency value, $\omega_b = 0.05\omega_{pe}$.

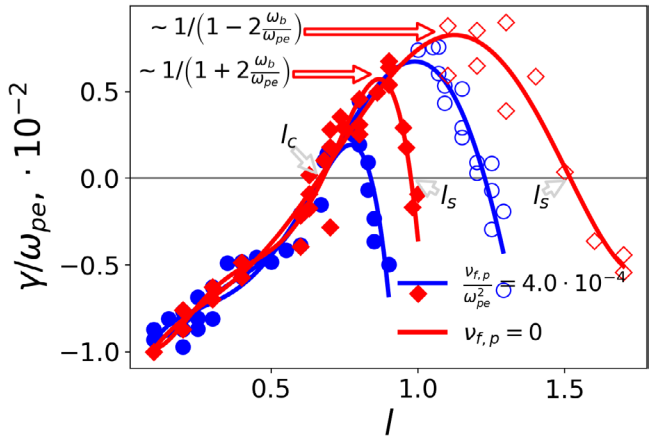

Figure 8. The normalized secondary mode growth/decay rate versus l in a pure diffusion case (diamond markers) and in the presence of drag (circle markers). Solid lines represent the best fit line for each case. The bounce frequency at the deeply trapped end, $\omega_b/\omega_{p,e} = 0.1$. The D_p and $\nu_{f,p}$ values and normalization have been chosen as in figures 5–7 ($D_p = 1.6\cdot10^{-5}\omega_{pe}^3$, $\nu_{f,p} = 4.0\cdot10^{-4}\omega_{pe}^2/0$). The regions of negative γ correspond to the stability regions of secondary modes.

COBBLES code in its full-f version (see in the appendix A.5) has been adopted to provide the numerical results. They are found to be in good agreement. The benchmarking details are given in the appendix A.5. $\omega_b \approx 0.15\omega_{pe}$ is approximately the point after which the comparison could no longer be provided. This corresponds to longer times, when the effects outside the secondary mode stability analysis start playing a role such as mode-mode coupling and the mode non-linear saturation.

5. Summary and conclusions

The purpose of the work presented here is to identify the conditions under which an island in phase space, formed by trapping of EPs in a plasma wave, is subject to secondary instabilities in the presence of collisions. This is a subject of relevance to MHD instabilities driven by EPs (EP-MHD) in tokamaks such as fishbones, TAEs or EP-driven geodesic

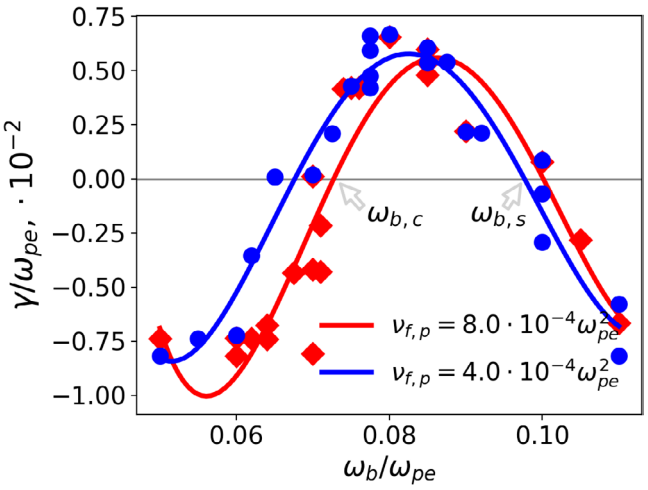

Figure 9. The normalized secondary mode growth/decay rate versus bounce frequency of deeply trapped particles, ω_b in the presence of drag, $\nu_{f,p}$ (solid lines represent the best fit line for each case). The p space diffusion is fixed, $D_p = 1.6 \cdot 10^{-5}\omega_{pe}^3$. The primary/secondary wave number ratio, $l = 1.25$. The D_p and $\nu_{f,p}$ normalization have been chosen as in figures 5–7. In each case arrows indicate roots of $\gamma = \gamma(\omega_b)$. The first root, $\omega_{b,c}$, corresponds to a critical island half-width, below which the secondary mode is stable. While the second root, $\omega_{b,s}$ defines a saturation level, above which the secondary mode stability is reached.

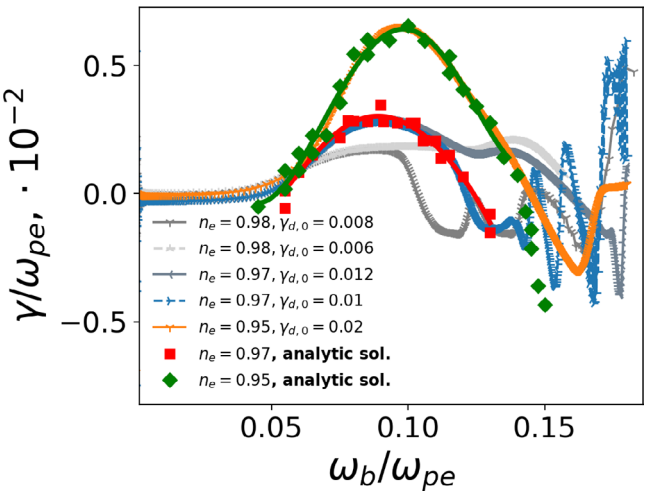

Figure 10. The secondary mode growth/decay rate against ω_b in a pure diffusion case, $D_p = 1.6 \cdot 10^{-5}\omega_{pe}^3$ (D_p value and normalization have been chosen as in figures 5–7). The primary/secondary mode number ratio, $k_0/k = 4/5$. An analytic solution (square and diamond markers) is calculated based on equations (51) and (52)/equation (53). Solid lines represent the COBBLES growth/decay rates.

acoustic modes (EGAMs). The particle dynamics in toroidal magnetic configurations is integrable and can be described by a set of action/angle variables in 6D phase space. A single Hamiltonian resonant perturbation generally leads to the formation of an island-like structure near the resonant surface. The dynamics in the vicinity of this island can be reduced to a 2D, parametrized by two invariants of motion that lie on the resonant surface. Hence, a single EP-MHD mode is interpreted as a reduced 2D Hamiltonian dynamics near the island in phase space.

A prototype of such dynamics is the bump-on-tail instability, which arises in 2D space, $\{position, velocity\}$. In the simplest version, the bump-on-tail instability is a Langmuir wave that becomes unstable when the electron/ion distribution function exhibits a positive slope near the resonant velocity. In the presence of strong enough dissipation, a single wave, called here the initial primary wave, evolves towards a steady island structure. The electron/ion distribution function, associated with the island, represents a 'perturbed' equilibrium. It has been computed here by solving the Fokker–Planck equation. We chose the collision operator as a combination of pitch angle scattering, velocity space diffusion and dynamical friction. The last term is not negligibly small for ITER like parameters and hence needs to be accounted for. The aforementioned dimensionality reduction from 6D to 2D allows the Fokker–Planck equation to be solved in the presence of tokamak plasma drifts, not focusing on the idealized purely electrostatic slab formulation. This 'perturbed' equilibrium includes a thin separatrix layer, where collisional effects balance the free streaming contribution and hence an expansion in the small ratio of the diffusion/drag coefficient to ω_b^3/ω_b^2 could no longer be applied. The dynamical friction results in a hole close to the island O-point, while diffusion controls the boundary layer near the separatrix. This numerical solution has been successfully benchmarked against an analytic solution that is valid in the case of vanishing dissipation, and also against the full-f kinetic COBBLES code. The steepening of the distribution function near the island separatrix opens the way to the emergence of secondary instabilities due to the strong positive gradient of the distribution function in velocity space in this boundary layer. The 'perturbed' equilibrium is a true non-linear state: a linear perturbative approach cannot be applied whenever the island width is significant. Thus, a stability analysis that fully accounts for nonlinearities due to the island shape has been developed, based on the action/angle approach and a variational form of the Maxwell equations. It leads to a tractable dispersion relation that we have analyzed numerically. The results have been compared with the full non-linear solution, provided by the COBBLES code. It has been found that the growth rate of a secondary mode is maximum when the associated resonant velocity approaches the boundary of the primary island, which was an expected result.

A key question in the context of EP-MHD modes is the loss of EPs, induced by the non-linear evolution of these modes. The bump-on-tail approach we use allows the EP losses to be found through the damping contribution of the Lagrangian of the primary/secondary modes as well as from the EP drive that comes from the slope of the distribution function within the island. Losses are related to the instability strength. In the limit of strong dissipation where the island width saturates, particle losses are moderate and controlled by the boundary layer near the separatrix. When dissipation is small, the distribution function exhibits structures in phase space that evolve in time. Losses are tied to this complex dynamics. One signature of this dynamics is frequency chirping, the explanation of which is still debated. In the limit of weak drive, the Berk–Breizman model is most commonly applied. It is based on the formation

of clump/hole pairs that move away from the resonant surface in phase space. Although their asymptotic dynamics is quite well understood, the formation process of these clump/hole pairs is not yet clear. Some recent works [16, 37] have proposed that secondary instabilities are triggered, which lead to the formation of fine scale structures in phase space, and finally to the production of clump/hole pairs.

Our results also can be compared with works [16, 37], where less dissipative solutions have been addressed. In the latter case, the distribution function evolves towards an unmodulated rectangular shape in velocity space, which is quite different from the island-like structure. As in [16, 37], a threshold in the width of the region where the distribution function flattens must be exceeded to see the appearance of secondary instabilities. The threshold found in [16, 37] cannot be quantitatively compared with the one found in this paper since it is dictated by the island width in the present work, while the plateau is unmodulated in the spatial direction in the low dissipation case. Nevertheless, the orders of magnitude are the same. One important result of the present study is the subharmonic character of the secondary wave compared with the primary mode. Secondary wave numbers are found to be smaller than the primary wave number in qualitative agreement with previous works on BGK mode stability. This may prevent the onset of a secondary wave if the primary wave number is already the lowest available. One may interpret this property as a certain robustness of an island-like structure in the presence of collisions, which would explain why no/slow chirping is observed in collisional situations. We also note that turbulence has been proposed as a mechanism that quenches clump/hole formation [28].

The present work is subject to some limitations. The radial mode structure [38, 39] has not been addressed in this paper. [39] shows that the narrow structure of the model Alfvén mode eigenfunction decreases the resonance island width and hence, in principle, can decrease the secondary mode stability threshold, $\omega_{b,c}$. In contrast, as stated above, the effect of drag increases the marginal island width. Hence, $\omega_{b,c}$ would be determined by a competition of these two effects. In addition, the effects of finite orbit width (FOW) and finite Larmor radius (FLR) of EPs on TAEs are left beyond the scope of the paper. Following [40], the FOW can be introduced perturbatively by Taylor expanding the electrostatic potential about the guiding centre provided the characteristic length scale of the variation of the electric field is larger than the Larmor radius. The FOW effects are shown to be stabilizing for TAEs localized in a plasma core and destabilizing for global TAEs at the tokamak edge [41]. Although the secondary instability onset has been demonstrated, it does not provide an explanation of the initial erosion of the island separatrix that ultimately leads to the asymptotic dynamics, proposed by Berk and Breizman. However, more rigorous derivations are required to provide the actual picture. Furthermore, the stability of a single phase space island has been investigated here, taking as an assumption that a single primary mode exists. In a tokamak for instance it corresponds to a single isolated EP-MHD mode. In a more general case, there can be a number of resonant primary harmonics. Resonating on the same rational surface, they maintain the island-like configuration, but deform the separatrix. In contrast, when harmonics resonate on different surfaces, several islands are formed and can overlap according to the Chirikov criterion. Inside the overlapping region, stochasticity is generated. The resulting transport can in principle flatten the distribution function between two adjacent rational surfaces and thus prevent secondary instabilities in the stochastic layer that is thus formed. According to some theories, this is relevant to a case in ITER advanced scenarios when several TAEs arise simultaneously. This situation is left for future work.

Acknowledgments

This work was funded by the University of York Overseas Research Scholarship and by the French Research Federation for Magnetic Fusion Studies. Computations were performed on the EXPLOR cluster. The authors would like to acknowledge the 9th Festival de Théorie in Aix-en-Provence, France, where this work was initiated. Also, the authors would like to thank J. Candy for a helpful discussion regarding this work.

Appendix

A.1. Primary equilibrium: numerical grid

The numerical solution technique for the Fokker–Planck equation, equation (14)/equation (18), with the matching conditions at the trapped/passing boundary, given in section 3, is presented in this appendix. This is a 2D/1D differential equation in $\{\xi, H_0; \sigma_p\} / \{H_0; \sigma_p\}$. The D_p and $\nu_{f,p}$ are taken as parameters. To provide the Maxwellian behavior far from the island in phase space, we require a zero p and hence H_0 gradient of $g_{0,j}$ at $p \to \pm\infty$. In ξ space, we simply impose $g_{0,j}(-\xi_b) = g_{0,j}(\xi_b)$ ($\xi_b = \pi$ for a branch of passing particles). To solve equation (14)/equation (18), we apply the shooting method in H_0 direction, reducing it to a matrix/algebraic equation for any H_0. Applying the finite difference scheme to H_0 space (central difference to the equation and forward/backward difference at the edges of H_0 space), we obtain the following matrix equation:

$$\boldsymbol{P}_j^\sigma \boldsymbol{g}_{j+1}^\sigma + \boldsymbol{Q}_j^\sigma \boldsymbol{g}_j^\sigma + \boldsymbol{R}_j^\sigma \boldsymbol{g}_{j-1}^\sigma + \boldsymbol{A}_j^\sigma = 0 \qquad \text{(A.1)}$$

for the vector solution, $\boldsymbol{g}_j$, we seek at each H_0 grid point, j (note: for equation (18) $\boldsymbol{g}_j$ becomes a scalar, g_j, and equation (A.1) should be understood as an algebraic at each j). $\sigma = \pm 1$ for the passing and $\sigma = |\sigma|$ for the trapped branches (note: $|\sigma|$ denotes $\pm 1/+1$ for the trapped branch of equation (14)/equation (18), respectively). $\boldsymbol{P}_j^\sigma$, $\boldsymbol{Q}_j^\sigma$ and $\boldsymbol{R}_j^\sigma$ are square diagonal matrices of size $N_\xi \times N_\xi$, and $\boldsymbol{A}_j^\sigma$ is the right hand side vector; both, $\boldsymbol{g}_j$ and $\boldsymbol{A}_j^\sigma$, are of length N_ξ (N_ξ is a number of points in ξ direction). For the reduced ξ-averaged Fokker–Planck equation, equation (18), all the coefficients in equation (A.1) as well as the right hand side become scalars. The left boundary in a general form in H_0 space (i.e. for deeply trapped particles at $j = 0$) reads

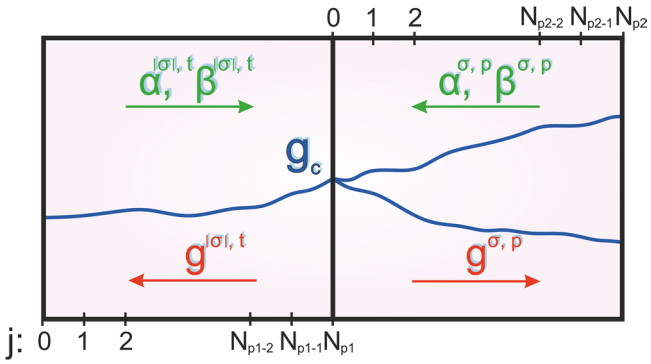

Figure A1. A schematic representation of the solution technique.

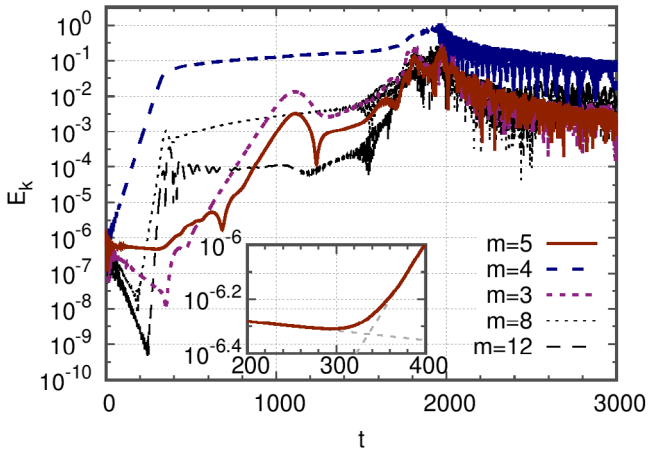

Figure A2. Time evolution of the amplitudes of Fourier modes $k = mk_1$ of the E-field. Inset: zoom near the time of reversal of evolution of the mode $m = 5$. In the inset, the two dashed lines correspond to growth/decay rates $\gamma_{5,L} = -0.0008$ and $\gamma_{5,\mathrm{sec}} = 0.012$. The diffusion and the slowing down rates are $\nu_{d,V} = 10^{-2}$ and $\nu_{f,V} = 0$, respectively.

$$\hat{\boldsymbol{P}}_0^{|\sigma|,t}\boldsymbol{g}_0^{|\sigma|,t} + \hat{\boldsymbol{Q}}_0^{|\sigma|,t}\boldsymbol{g}_1^{|\sigma|,t} + \hat{\boldsymbol{R}}_0^{|\sigma|,t}\boldsymbol{g}_2^{|\sigma|,t} + \hat{\boldsymbol{A}}_0^{|\sigma|,t} = 0. \tag{A.2}$$

To set the $j = 0$th element, we assume a linear relation between $\boldsymbol{g}$ at jth and $(j+1)$th grid points, and hence we write

$$\boldsymbol{g}_j^{|\sigma|,t} = \boldsymbol{\alpha}_j^{|\sigma|,t}\boldsymbol{g}_{j+1}^{|\sigma|,t} + \boldsymbol{\beta}_j^{|\sigma|,t}, \tag{A.3}$$

from the side of trapped particles. Here $\boldsymbol{\alpha}_j^{|\sigma|,t}$ is the square matrix and $\boldsymbol{\beta}_j^{|\sigma|,t}$ is a vector of length N_ξ. Combining equations (A.1) and (A.3), we obtain the following recurrence relation:

$$\begin{aligned}\boldsymbol{\alpha}_j^{|\sigma|,t} &= -\left[\boldsymbol{Q}_j^{|\sigma|,t} + \boldsymbol{R}_j^{|\sigma|,t}\boldsymbol{\alpha}_{j-1}^{|\sigma|,t}\right]^{-1}\boldsymbol{P}_j^{|\sigma|,t},\\ \boldsymbol{\beta}_j^{|\sigma|,t} &= -\left[\boldsymbol{Q}_j^{|\sigma|,t} + \boldsymbol{R}_j^{|\sigma|,t}\boldsymbol{\alpha}_{j-1}^{|\sigma|,t}\right]^{-1}\left[\boldsymbol{R}_j^{|\sigma|,t}\boldsymbol{\beta}_{j-1}^{|\sigma|,t} + \boldsymbol{A}_j^{|\sigma|,t}\right].\end{aligned} \tag{A.4}$$

Combining equations (A.2)–(A.4), we calculate $\boldsymbol{\alpha}_0^{|\sigma|,t}$ and $\boldsymbol{\beta}_0^{|\sigma|,t}$ at the deeply trapped end. Then using equation (A.4) we find all $\boldsymbol{\alpha}_j^{|\sigma|,t}$s with $\boldsymbol{\beta}_j^{|\sigma|,t}$s up to the trapped/passing boundary, $H_0 = H_0^c$ $(j = N_{p1})$, as shown in figure A1. We apply the exact same algorithm to the passing branch. The right boundary condition, i.e. for deeply passing particles at $j = N_{p2}$, is

$$\hat{\boldsymbol{P}}_{N_{p2}}^{\sigma,p}\boldsymbol{g}_{N_{p2}}^{\sigma,p} + \hat{\boldsymbol{Q}}_{N_{p2}}^{\sigma,p}\boldsymbol{g}_{N_{p2}-1}^{\sigma,p} + \hat{\boldsymbol{R}}_{N_{p2}}^{\sigma,p}\boldsymbol{g}_{N_{p2}-2}^{\sigma,p} + \hat{\boldsymbol{A}}_{N_{p2}}^{\sigma,p} = 0. \tag{A.5}$$

Employing

$$\boldsymbol{g}_j^{\sigma,p} = \boldsymbol{\alpha}_j^{\sigma,p}\boldsymbol{g}_{j-1}^{\sigma,p} + \boldsymbol{\beta}_j^{\sigma,p}, \tag{A.6}$$

and substituting this into the initial equation, equation (A.1), we come to

$$\begin{aligned}\boldsymbol{\alpha}_j^{\sigma,p} &= -\left[\boldsymbol{P}_j^{\sigma,p}\boldsymbol{\alpha}_{j+1}^{\sigma,p} + \boldsymbol{Q}_j^{\sigma,p}\right]^{-1}\boldsymbol{R}_j^{\sigma,p},\\ \boldsymbol{\beta}_j^{\sigma,p} &= -\left[\boldsymbol{P}_j^{\sigma,p}\boldsymbol{\alpha}_{j+1}^{\sigma,p} + \boldsymbol{Q}_j^{\sigma,p}\right]^{-1}\left[\boldsymbol{P}_j^{\sigma,p}\boldsymbol{\beta}_{j+1}^{\sigma,p} + \boldsymbol{A}_j^{\sigma,p}\right].\end{aligned} \tag{A.7}$$

Combining equations (A.5)–(A.7), we calculate $\boldsymbol{\alpha}_{N_{p2}}^{\sigma,p}$ and $\boldsymbol{\beta}_{N_{p2}}^{\sigma,p}$ at the deeply passing end and using equation (A.7) we find all $\boldsymbol{\alpha}_j^{\sigma,p}$s with $\boldsymbol{\beta}_j^{\sigma,p}$s up to $H_0 = H_0^c$ $(j = 0)$ from the passing side (see figure A1). Once all $\boldsymbol{\alpha}_j^{\sigma}$s and $\boldsymbol{\beta}_j^{\sigma}$s are obtained from the passing and the trapped side (the trapped/passing boundary itself, $j = N_{p1}$ for trapped and $j = 0$ for passing particles, is excluded from the scheme), we apply the matching conditions, introduced in section 3. To solve equation (14), we require both σ branches of the solution we seek to be in a class $\boldsymbol{C}^1$ (i.e. $\sum_\sigma \sigma g^{\sigma,p} = \sum_{|\sigma|}|\sigma|\, g^{|\sigma|,t}$, $\sum_\sigma g^{\sigma,p} = \sum_{|\sigma|} g^{|\sigma|,t}$ and similar relations for the first derivatives), which translates into

$$\begin{aligned}&\boldsymbol{g}_0^{+1,p} = \boldsymbol{g}_0^{+1,t} \equiv \boldsymbol{g}_c^{+},\\ &\boldsymbol{g}_0^{-1,p} = \boldsymbol{g}_0^{-1,t} \equiv \boldsymbol{g}_c^{-},\\ &\frac{1}{\Delta H_{0,t}}\left[3\boldsymbol{g}_{N_{p1}}^{+1,t} - 4\boldsymbol{g}_{N_{p1}-1}^{+1,t} + \boldsymbol{g}_{N_{p1}-2}^{+1,t} + 3\boldsymbol{g}_{N_{p1}}^{-1,t} - 4\boldsymbol{g}_{N_{p1}-1}^{-1,t} + \boldsymbol{g}_{N_{p1}-2}^{-1,t}\right]\\ &= \frac{1}{\Delta H_{0,p}}\left[-\boldsymbol{g}_2^{+1,p} + 4\boldsymbol{g}_1^{+1,p} - 3\boldsymbol{g}_0^{+1,p} - \boldsymbol{g}_2^{-1,p} + 4\boldsymbol{g}_1^{-1,p} - 3\boldsymbol{g}_0^{-1,p}\right],\\ &\frac{1}{\Delta H_{0,t}}\left[3\boldsymbol{g}_{N_{p1}}^{+1,t} - 4\boldsymbol{g}_{N_{p1}-1}^{+1,t} + \boldsymbol{g}_{N_{p1}-2}^{+1,t} - 3\boldsymbol{g}_{N_{p1}}^{-1,t} + 4\boldsymbol{g}_{N_{p1}-1}^{-1,t} - \boldsymbol{g}_{N_{p1}-2}^{-1,t}\right]\\ &= \frac{1}{\Delta H_{0,p}}\left[-\boldsymbol{g}_2^{+1,p} + 4\boldsymbol{g}_1^{+1,p} - 3\boldsymbol{g}_0^{+1,p} + \boldsymbol{g}_2^{-1,p} - 4\boldsymbol{g}_1^{-1,p} + 3\boldsymbol{g}_0^{-1,p}\right]\end{aligned} \tag{A.8}$$

to find the boundary elements, $\boldsymbol{g}_c^{\pm}$. The uniform grid has been assumed here, $\Delta H_{0,p,t}$ are the step sizes in H_0 space for the passing and trapped branches, respectively. For the reduced Fokker–Planck equation, equation (18), whose trapped solution is σ-independent due to ξ averaging, the matching conditions at H_0^c reduce to $\sum_\sigma \sigma g^{\sigma,p} = 0$, $\sum_\sigma g^{\sigma,p} = 2g^{|\sigma|,t}$ and $\sum_\sigma \partial g^{\sigma,p}/\partial H_0 = 2\partial g^{|\sigma|,t}/\partial H_0$ that translate into

$$\begin{aligned}&g_{N_{p1}}^{|\sigma|,t} = g_0^{+1,p} = g_0^{-1,p} \equiv g_c,\\ &\frac{2}{\Delta H_{0,t}}\left[3g_{N_{p1}}^{|\sigma|,t} - 4g_{N_{p1}-1}^{|\sigma|,t} + g_{N_{p1}-2}^{|\sigma|,t}\right]\\ &= \frac{1}{\Delta H_{0,p}}\left[-g_2^{+1,p} + 4g_1^{+1,p} - 3g_0^{+1,p} - g_2^{-1,p} + 4g_1^{-1,p} - 3g_0^{-1,p}\right],\end{aligned} \tag{A.9}$$

to find the boundary element, g_c. Substituting equations (A.3) and (A.6) into (A.8)/equation (A.9) gives us a relation for $\boldsymbol{g}_c^{\pm}/g_c$. Once $\boldsymbol{g}_c^{\pm}/g_c$ is found, we reconstruct the rest solution elements from equations (A.3) and (A.6) up to the trapped/passing edges. The described solution technique is illustrated in figure A1 for equation (18).

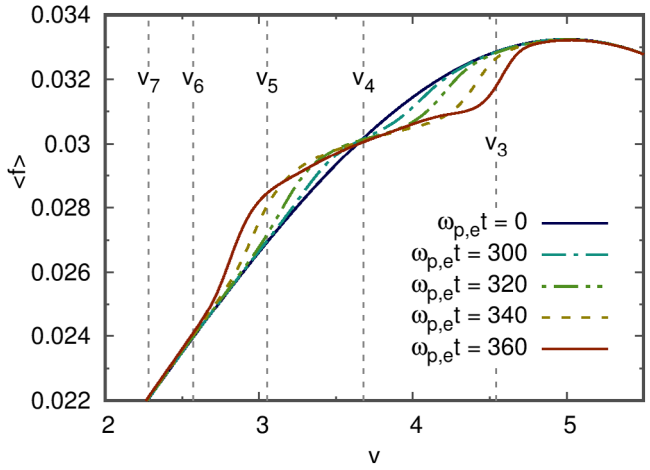

Figure A3. Spatial average of the distribution function. Vertical lines indicate phase velocities $V_m = \omega_{m,L0}$ of modes $k_m = mk_1$. The diffusion and the slowing down rates are $\nu_{d,V} = 10^{-2}$ and $\nu_{f,V} = 0$, respectively.

A.2. Resonant and non-resonant representation of the dispersion relation

To show that both resonant equations (51) and (52) and non-resonant equation (53), representations of the dispersion function are equivalent, we compare resonant parts of the perturbed distribution function, $g_{j\omega}$, given by equations (34)/(39),(40) and (45), (47). Substituting equations (47) and (49) into (45) gives

$$g_{j\omega}(\alpha, H_0; \sigma_p) = -\sum_{n\in\mathbb{Z}} \frac{\delta\omega}{\delta\omega - n\Omega_b + \mathrm{i}0^+} \frac{\partial f_{0,j}}{\partial H_0} h_{k\omega} \mathrm{e}^{\mathrm{i}n\alpha} \int_{-\pi}^{\pi} \frac{\mathrm{d}\alpha'}{2\pi} \mathrm{e}^{\mathrm{i}\left(l\xi' - n\alpha'\right)}. \tag{A.10}$$

Using the Landau relation, which is

$$\frac{1}{\delta\omega - n\Omega_b + \mathrm{i}0^+} = -\mathrm{i}\int_{\mathbb{R}^+} \mathrm{e}^{\mathrm{i}(\delta\omega - n\Omega_b)\sigma} \mathrm{d}\sigma, \tag{A.11}$$

and then applying the Shah function relation:

$$\sum_{n\in\mathbb{Z}} \mathrm{e}^{\mathrm{i}n\left(\alpha - \alpha' - \Omega_b\sigma\right)} = 2\pi \sum_{k\in\mathbb{Z}} \delta\left(\alpha - \alpha' - \Omega_b\sigma - 2\pi k\right) \tag{A.12}$$

we modify the above formula to obtain

$$g_{j\omega}(\alpha, H_0; \sigma_p) = 2\pi\mathrm{i}\delta\omega \frac{\partial f_{0,j}}{\partial H_0} h_{k\omega} \sum_{n\in\mathbb{Z}} \int_{\mathbb{R}^+} \mathrm{d}\sigma \int_{-\pi}^{\pi} \frac{\mathrm{d}\alpha'}{2\pi} \mathrm{e}^{\mathrm{i}\left(l\xi' + \delta\omega\sigma\right)} \delta\left(\alpha - \alpha' - \Omega_b\sigma - 2\pi n\right), \tag{A.13}$$

which we can rewrite as

$$g_{j\omega}(\alpha, H_0; \sigma_p) = 2\pi\mathrm{i}\frac{\delta\omega}{\Omega_b} \frac{\partial f_{0,j}}{\partial H_0} h_{k\omega} \sum_{n\in\mathbb{Z}} \int_{-\pi/2}^{3\pi/2} \frac{\mathrm{d}\alpha'}{2\pi} \exp\left[\mathrm{i}\left(l\xi' + \delta\omega\frac{\alpha - \alpha' + 2\pi n}{\Omega_b}\right)\right] \cdot \Theta\left(\frac{\alpha - \alpha' + 2\pi n}{\Omega_b}\right). \tag{A.14}$$

Here we have used a limit operation for a periodic function to change the limits of integration, and n has been replaced by $-n$ due to periodicity. δ and Θ are used for the Dirac delta and the Heaviside step functions, respectively. From now we assume $\Omega_b > 0$, the same analysis can be produced for negative Ω_b values. As $\alpha, \alpha' \in [-\pi/2; 3\pi/2]$, $\alpha - \alpha' \in [-2\pi; 2\pi]$. For $n \leqslant -1$ the Heaviside function is always zero. If $n = 0$, then $\alpha' \in [-\pi/2; \alpha]$. If $n = 1$, the Θ-function is always one. Therefore,

$$g_{j\omega}(\alpha, H_0; \sigma_p) = 2\pi\mathrm{i}\frac{\delta\omega}{\Omega_b} \frac{\partial f_{0,j}}{\partial H_0} h_{k\omega} \int_{-\pi/2}^{\alpha} \frac{\mathrm{d}\alpha'}{2\pi} \exp\left[\mathrm{i}\left(l\xi' + \delta\omega\frac{\alpha - \alpha'}{\Omega_b}\right)\right] + 2\pi\mathrm{i}\frac{\delta\omega}{\Omega_b} \frac{\partial f_{0,j}}{\partial H_0} h_{k\omega} \sum_{n=1}^{+\infty} \int_{-\pi}^{\pi} \frac{\mathrm{d}\alpha'}{2\pi} \exp\left[\mathrm{i}\left(l\xi' + \delta\omega\frac{\alpha - \alpha' + 2\pi n}{\Omega_b}\right)\right]. \tag{A.15}$$

Applying equation (41), we obtain

$$g_{j\omega}(\alpha, H_0; \sigma_p) = 2\pi\mathrm{i}\frac{\delta\omega}{\Omega_b} \frac{\partial f_{0,j}}{\partial H_0} h_{k\omega} \left\{ \int_{-\pi/2}^{\alpha} \frac{\mathrm{d}\alpha'}{2\pi} \exp\left[\mathrm{i}\left(l\xi' + \delta\omega\frac{\alpha - \alpha'}{\Omega_b}\right)\right] + \frac{\int_{-\pi}^{\pi} \frac{\mathrm{d}\alpha'}{2\pi} \exp\left[\mathrm{i}\left(l\xi' + \delta\omega\frac{\alpha - \alpha'}{\Omega_b}\right)\right]}{\exp\left(-2\pi\mathrm{i}\frac{\delta\omega}{\Omega_b}\right) - 1} \right\}, \tag{A.16}$$

which is exactly equations (39) and (40).

A.3. Wave-particle energy exchange

To calculate energy exchanged between waves and particles, δW, we need to address the imaginary part of the Lagrangian, given by equation (6). Hence, using the final dispersion relation, equation (51), we write $\delta W = -2\delta\omega\Im D|h_{k\omega}|^2$. Applying the Sokhotski–Plemelj formula, $\frac{1}{\delta\omega - n\Omega_b \pm \mathrm{i}0^+} = p\cdot V\cdot \frac{1}{\delta\omega - n\Omega_b} \mp \mathrm{i}\pi\delta\left(\delta\omega - n\Omega_b\right)$ to real $\delta\omega$, we come to

$$\delta W = -2\pi\omega_{pj}^2\delta\omega \sum_{n=-\infty}^{+\infty} n\sum_{\sigma_p} \int_{-\omega_b^2}^{+\infty} \mathrm{d}H_0 \frac{\partial f_{0,j}}{\partial H_0} |h_{n\omega}|^2 \delta\left(\delta\omega - n\Omega_b\right). \tag{A.17}$$

This energy exchange is negative, provided $\frac{\partial f_{0,j}}{\partial H_0} > 0$, i.e. the secondary mode drive is possible, which we could see from the secondary mode stability analysis.

A.4. Angle variable for trapped and passing particles

It is convenient to introduce a trapped parameter defined as

$$\kappa^2 = \frac{2\omega_b^2}{H_0 + \omega_b^2}. \tag{A.18}$$

The passing domain corresponds to $0 \leqslant \kappa \leqslant 1$, while the trapped domain is determined by $1 \leqslant \kappa < +\infty$. The bounce frequency is then given by the relation $\Omega_b = 1/2\tau(\kappa)$ for trapped and by $\Omega_b = \sigma_p/2\tau(\kappa)$ for passing particles, where the function τ is such that

$$\tau(\kappa) = \frac{2}{\pi} K\left(\kappa^2\right), \quad 0 \leqslant \kappa \leqslant 1$$
$$\tau(\kappa) = \frac{2}{\pi}\frac{1}{\kappa} K\left(\frac{1}{\kappa^2}\right), \quad 1 \leqslant \kappa < +\infty. \tag{A.19}$$

Here K is the complete elliptic integral of the first kind. As expected, the bounce/transit period becomes large near the trapped/passing boundary, $\kappa = 1$, since $K(\kappa) \simeq -\frac{1}{2}\ln|1 - \kappa|$ for $|1 - \kappa| \ll 1$. A useful expression for α in the upper quadrant $0 \leqslant \xi \leqslant \pi/2$, $0 \leqslant \alpha \leqslant \pi/2$ is

$$\alpha = \frac{F\left(\xi/2, \kappa^2\right)}{F\left(\pi/2, \kappa^2\right)}, \quad 0 \leqslant \kappa \leqslant 1$$
$$\alpha = \frac{\pi}{2}\frac{F\left(\sin^{-1}\left[\kappa \sin\left(\xi/2\right)\right], \kappa^{-2}\right)}{F\left(\pi/2, \kappa^{-2}\right)}, \quad 1 \leqslant \kappa < +\infty. \tag{A.20}$$

Here F is the incomplete elliptic function of the first kind, defined as $F(\delta, m) = \int_0^\delta \frac{\mathrm{d}\delta'}{\sqrt{1-m\sin^2\delta'}}$. This relation can formally be inverted to provide a link between the angles ξ and α. Using the relation between complete and incomplete elliptic integrals, $K(m) = F(\pi/2, m)$, we rewrite equation (A.19) as

$$\sin\left(\frac{\xi}{2}\right) = sn\left(\frac{\tau\alpha}{2}, \kappa^2\right), \quad 0 \leqslant \kappa \leqslant 1$$
$$\sin\left(\frac{\xi}{2}\right) = \frac{1}{\kappa} sn\left(\kappa\tau\alpha, \frac{1}{\kappa^2}\right), \quad 1 \leqslant \kappa < +\infty \tag{A.21}$$

valid for all αs and ξs. The function $sn(\delta, m)$ is the Jacobian elliptic function that coincides with the trigonometric $\sin\delta$ for $m \leqslant 1$. One recovers that $\xi = \alpha$ for deeply passing particles $\kappa = 0$, and $\xi = \xi_0 \sin\alpha$ for deeply trapped particles $\kappa \to \infty$. ξ_0 here is the bounce angle, $\sin(\xi_0/2) = 1/\kappa$. Note however that the function differs significantly from the sine function for barely trapped and passing particles $\kappa \sim 1$.

A.5. COBBLES simulation

The primary equilibrium distribution function and the secondary mode growth/decay rate, based on equations (51) and (52)/equation (53), have been benchmarked against the COBBLES code, which is to be described in this appendix.

We cast the Berk–Breizman model [29] in a many-wave form. We consider a 1D plasma with a distribution function, $f(t, x, V)$, in a box length $L = 2\pi/k_1$ with periodic boundary conditions in x direction (k_1 is the lower secondary mode number). To ensure quasineutrality, we assume a background population of the opposite charge with a distribution function $\bar{f}(t, V)$, which is the spatial average of f. In the initial condition, the velocity distribution,

$$f_0(V) \equiv \bar{f}(t=0, V) = f_0^{e,i}(V) + f_0^{\mathrm{fe,fi}}(V), \tag{A.22}$$

comprises a Maxwellian bulk,

$$f_0^{e,i}(V) = \frac{n_{e,i}}{V_{Te,i}\sqrt{2\pi}} \mathrm{e}^{-\frac{1}{2}\left(\frac{V}{V_{Te,i}}\right)^2}, \tag{A.23}$$

and a beam of high energy particles,

$$f_0^{\mathrm{fe,fi}}(V) = \frac{n_{\mathrm{fe,fi}}}{V_{T\mathrm{fe,fi}}\sqrt{2\pi}} \mathrm{e}^{-\frac{1}{2}\left(\frac{V-V_b}{V_{T\mathrm{fe,fi}}}\right)^2}, \tag{A.24}$$

where $n_{e,i}$ and $n_{\mathrm{fe,fi}}$ are bulk and beam electron/ion densities, $V_{Te,i}$ and $V_{T\mathrm{fe,fi}}$ are thermal velocities of bulk and beam particles, and V_b is the electron/ion beam drift velocity. The evolution of a full electron/ion distribution is described by equation (4), coupled to the displacement current equation (DCE),

$$\frac{\partial E}{\partial t} = -\frac{eZ_j}{\varepsilon_0}\int V(f - f_0)\,\mathrm{d}V - 2\gamma_d E, \tag{A.25}$$

to provide self-consistency. The DCE is used here instead of Poisson's equation to find the time dependent E-field, $E = -\partial\Phi/\partial x$. γ_d is the ad-hoc damping rate, defined as in [25]. In the limit of $\gamma_d = 0$, equation (A.25) is equivalent to Poisson's equation. The average electric field, E_0, is kept zero at all times. The term proportional to γ_d is an external wave damping, which is taken to be model for all linear dissipative mechanisms of the wave energy to the background plasma [31]. Note that unlike previous works, γ_d is allowed to depend on the wave number. Due to periodicity in x, we seek a solution, written as a Fourier series in x such that $E(x,t) = E_k(t)\,\mathrm{e}^{\mathrm{i}kx} + \mathrm{c.c.}$ and similarly for f. Here we have assumed a single mode of the wave number k, which corresponds to the situation of an isolated single TAE. For $k \neq 0$, equation (A.25) yields the time evolution of the wave. In the initial condition we apply small perturbations, $f(t=0, x, V) = f_0(V)\left[1 + \sum_k \epsilon_k \cos(kx + \phi_k)\right]$, where each ϕ_k is a random phase. The initial value of E is obtained by solving Poisson's equation. The right hand side of equation (4) is the adopted 1D projection of the Fokker–Planck operator [24, 30] that includes both drag and diffusion. It is given by equation (12), rewritten in V space.

To perform numerical simulations of the Berk–Breizman model, equations (4), (12) and (A.25), we adopt the COBBLES code in its full-f version (COBBLES stands for COnservative Berk–Breizman semi-Lagrangian Extended Solver). It has been developed in previous works [8, 32–34], based on the cubic-interpolated-propagation (CIP) scheme [35] and the Strang splitting method [36]. The normalization is as follows: time is normalized to the total electron/ion plasma frequency ω_p, distance to the smaller secondary wave number k_1, density to the total plasma density n_{eqm}, and electric field to $m_j\omega_p^2/(eZ_jk_1)$, where $\omega_p^2 = n_{eqm}eZ_j^2/(\varepsilon_0 m_j)$. All quantities like f are sampled on uniform Eulerian grids with N_x and N_V grid points in x and V directions, respectively, within the computational domain $\{(x,V)|\,0 \leqslant x < L = 2\pi/k_1, V_{min} \leqslant V \leqslant V_{\max}\}$. The boundary conditions are periodic in x direction and fixed in V direction. For the simulation, we have chosen $V_{\min} = -8, V_{\max} = 18$, $N_x = 256$, $N_V = 2048$ and a time step width $\Delta t = 0.05$. The simulated species is thermal electrons with the fast electron component included, and the ions act as a neutralizing species (the opposite situation is also allowed). To benchmark the solution of equation (14), which is localized to the island vicinity, against the COBBLES solution, valid in a full range of V, we need to set the $f_{0,j}$ behavior far from the island, i.e. $\partial f_{eqm}/\partial p|_{\mathrm{res}}$. As equation (4) is written in the absence of plasma drifts, p here needs to be understood as $k_0 V$. Provided p is normalized to ω_{pe}, $\omega_{pe}\,\partial f_{eqm}/\partial p|_{\mathrm{res}}$, which is equal to $\omega_{pe}\,\partial f_{eqm}/k_0\partial V|_{V_{\mathrm{ph}}}$, reads

$$\frac{1}{\sqrt{2\pi}\widehat{V}_{T\mathrm{fe}}} \mathrm{e}^{-\frac{1}{2}\left(\frac{\widehat{V}_{\mathrm{ph}}-\widehat{V}_b}{\widehat{V}_{T\mathrm{fe}}}\right)^2} \frac{\widehat{V}_b - \widehat{V}_{\mathrm{ph}}}{\widehat{V}_{T\mathrm{fe}}^2}$$

in units of $n_{\mathrm{fe}}k_0/\omega_{pe}$. Hats here indicate that the corresponding quantities have been normalized to ω_{pe}/k_0. The parameters for the initial bump-on-tail distribution are $V_{T\mathrm{fe}} = 0.72\omega_{pe}/k_0$, $V_b = 1.2\omega_{pe}/k_0$, $V_{\mathrm{ph}} = 0.9364\omega_{pe}/k_0 \approx \omega_{pe}/k_0$ and $n_{\mathrm{fe}}/n_{eqm} = 0.05$.

The COBBLES distribution function results are shown in figures 5–7 and are found to be in agreement with the localized solution in the vicinity of the phase space island. The dissipation is arbitrary set-up such that only one mode, namely mode $m=4$ (with $k_m = mk_1$), is linearly unstable for $f=f_0$. We choose $\gamma_d(k_4) = 0$ and $\gamma_d(k) = 0.038$ for $k \neq k_4$. We define $\omega_{m,L0}$ and $\gamma_{m,L0}$ as the linear frequency and growth rate of the mode of wave number $k_m = mk_1$ in the absence of dissipation and collisions. Note that $\gamma_{m,L0}$ is proportional to the slope of f_0 at the resonant velocity $V_m = \omega_{m,L0}/k_m$, $\gamma_{m,L0} = (\pi/2)\,\partial f_0/\partial V|_{V_m}$. We define the full linear growth rate $\gamma_{m,L}$ as the linear growth rate including the effects of collisions and dissipation. In the collisionless limit, when $\gamma_{m,L} \ll \omega_{m,L0}$, the full linear growth rate reduces to $\gamma_{m,L} = \gamma_{m,L0} - \gamma_d(k_m)$. With the parameters listed above, $\gamma_{4,L} = 0.034$ and $\gamma_{m,L} < 0$ for all $m \neq 4$. In particular, $\gamma_{3,L} = -0.009$ and $\gamma_{5,L} = -0.0008$. Figure A2 shows the time evolution of the amplitudes of modes $m=3$, 4, 5, 8 and 12, which are the dominant modes for the time interval $t<1000$. Figure A3 shows snapshots of the velocity distribution near the phase velocities of modes $m=3$, 4 and 5. We observe that mode $m=4$ grows linearly up to $t \approx 300$, after that it saturates. By comparing this with a control simulation, where all other ($m \neq 4$) modes are artificially filtered out, we have observed that the time evolution of both amplitude and velocity distribution are not significantly impacted by the presence of other modes until ~ 1000. Modes $m=5$ and $m=3$ decay linearly until $t \approx 200$ and $t \approx 320$, respectively, after that they grow. This timing of reversal coincides with the time when the steep slopes at the boundaries of the BGK island, formed by mode $m=4$, reach the phase velocities of modes $m=3$ and $m=5$. These results are qualitatively consistent with the secondary instability theory. As can be seen in figure A2, the growth rate of $m=5$ varies continuously around $t=300$. However, it does stabilize at $g_{5,\mathrm{sec}} = 0.012$ for a finite time interval, $380 < t < 400$. Figure A2 includes the amplitudes of modes 8 and 12. Since they are harmonics of the dominant mode $m=4$ and since the growth rate of $m=8$ is double that of $m=4$, we interpret their growth as the result of the fluid-like mode-mode coupling (probably in a class of modular-parametric instabilities), rather than the result of kinetic interactions between particles and waves. In the simulations of figures A2 and A3, the primary mode would be in a regime of constant-amplitude steady-state, if the secondary modes were not present. It is only in the presence of the other modes (including secondary instabilities), that the regime changes to a chaotic regime with strong amplitude oscillations and some chirping.

ORCID iDs

A.V. Dudkovskaia https://orcid.org/0000-0001-6890-3079
X. Garbet https://orcid.org/0000-0001-5730-1259
M. Lesur https://orcid.org/0000-0001-9747-5616
H.R. Wilson https://orcid.org/0000-0003-3333-7470

References

[1] Berk H.L., Breizman B.N. and Pekker M. 1996 *Phys. Rev. Lett.* **76** 1256
[2] Berk H.L., Breizman B.N. and Petviashvili N.V. 1997 *Phys. Lett.* A **234** 213
[3] Chen L. and Zonca F. 2016 *Rev. Mod. Phys.* **88** 015008
[4] Berk H.L. and Breizman B.N. 1990 *Phys. Fluids B* **2** 2226
[5] Berk H.L. and Breizman B.N. 1990 *Phys. Fluids* B **2** 2235
[6] Berk H.L. and Breizman B.N. 1990 *Phys. Fluids* B **2** 2246
[7] Vann R.G.L., Dendy R.O., Rowlands G., Arber T.D. and dÁmbrumenil N. 2003 *Phys. Plasmas* **10** 623
[8] Lesur M., Idomura Y. and Garbet X. 2009 *Phys. Plasmas* **16** 092305
[9] Zakharov V.E. and Karpman V.I. 1962 *Zh. Eksp. Teor. Fiz.* **43** 490 (in Russian); Zakharov V.E. and Karpman V.I. 1963 *Sov. Phys.—JETP* **16** 351
[10] O'Neil T. 1965 *Phys. Fluids* **8** 2255
[11] Mazitov R.K. 1965 *Zh. Prikl. Mekh. Tekh. Fiz.* **1** 27
[12] Galeev A.A. and Sagdeev R.S. 1973 *Rev. Plasma Phys.* **7** 1
[13] Wong K.-L. 1999 *Plasma Phys. Control. Fusion* **41** R1
[14] Berk H.L. *et al* 2006 *Nucl. Fusion* **46** S888
[15] Breizman B.N. and Sharapov S.E. 2011 *Plasma Phys. Control. Fusion* **53** 054001
[16] Lilley M.K. and Nyqvist R.M. 2014 *Phys. Rev. Lett.* **112** 155002
[17] Balmforth N.J. 2012 *Commun. Nonlinear Sci. Numer. Simul.* **17** 1989
[18] Bernstein B., Greene J.M. and Kruskal M.D. 1957 *Phys. Rev.* **108** 546
[19] Guo Y. and Strauss W.A. 1995 *Commun. Pure Appl. Math.* **63** 861
[20] Ghizzo A. *et al* 1988 *Phys. Fluids* **31** 72
[21] Manfredi G. and Bertrand P. 2000 *Phys. Plasmas* **7** 2425
[22] White R.B., Spizzo G. and Gobbin M. 2013 *Plasma Phys. Control. Fusion* **55** 115002
[23] Berk H.L., Breizman B.N. and Pekker M.S. 1997 *Plasma Phys. Rep.* **23** 778–88
[24] Lilley M.K., Breizman B.N. and Sharapov S.E. 2009 *Phys. Rev Lett.* **102** 195003
[25] Berk H.L. *et al* 1999 *Phys. Plasmas* **6** 3102
[26] Dudkovskaia A.V., Garbet X., Lesur M. and Wilson H.R. 2018 *J. Phys.: Conf. Ser.* **1125** 012009
[27] Wilson H.R., Connor J.W., Hastie R.J. and Hegna C.C. 1996 *Phys. Plasmas* **3** 248–65
[28] Woods B.J.Q., Duarte V.N., De-Gol A.P., Gorelenkov N.N. and Vann R.G.L. 2018 *Nucl. Fusion* **58** 082015
[29] Berk H.L., Breizman B.N. and Ye H. 1993 *Phys. Fluids* B **5** 1506
[30] Lesur M. *et al* 2010 *Phys. Plasmas* **17** 122311
[31] Berk H.L., Breizman B.N. and Pekker M. 1995 *Phys. Plasmas* **2** 3007
[32] Lesur M., Idomura Y. and Tokuda S. 2007 Kinetic simulations of electrostatic plasma waves using cubic-interpolated-propagation scheme *Report* 2006-089 (Japan Atomic Energy Agency)
[33] Lesur M. and Idomura Y. 2012 *Nucl. Fusion* **52** 094004
[34] Lesur M., Diamond P.H. and Kosuga Y. 2014 *Plasma Phys. Control. Fusion* **56** 075005
[35] Nakamura T. and Yabe T. 1999 *Comput. Phys. Commun.* **120** 122
[36] Strang G. 1968 *SIAM J. Numer. Anal.* **5** 506
[37] Eriksson F., Nyqvist R.M. and Lilley M.K. 2015 *Phys. Plasmas* **22** 092126
[38] Wang X. and Briguglio S. 2016 *New J. Phys.* **18** 085009
[39] White R.B., Gorelenkov N.N., Duarte V.N. and Berk H.L. 2018 *Phys. Plasmas* **25** 102504
[40] Fulop T., Lisak M., Kolesnichenko Y.I. and Anderson D. 1996 *Plasma Phys. Control. Fusion* **38** 811–28
[41] Gorelenkov N.N., Cheng C.Z. and Fu G.Y. 1999 *Phys. Plasmas* **6** 2802